Icarus 217 (2012) 297–314

Contents lists available at SciVerse ScienceDirect

Icarus

journal homepage: www.elsevier.com/locate/icarus

Searching for evidence of hydrothermal activity at Apollinaris Mons, Mars

M. Ramy El Maarry [a,b,*], James M. Dohm [c], Giuseppe A. Marzo [d], Robin Fergason [e], Walter Goetz [a], Essam Heggy [f], Andreas Pack [b], Wojciech J. Markiewicz [a]

[a] Max-Planck Institut für Sonnensystemforschung, Max-Planck Str., 2, 37191 Katlenburg-Lindau, Germany
[b] Universität Göttingen, Geowissenschaftliches Zentrum, Goldschmidtstrasse 1, 37077 Göttingen, Germany
[c] Department of Hydrology and Water Resources, University of Arizona, Tucson, AZ 85721, USA
[d] ENEA, C.R. Casaccia, via Anguillarese 301, 00123 S. Maria di Galeria, Roma, Italy
[e] Astrogeology Science Center, United States Geological Survey, 2255 N. Gemini Drive, Flagstaff, AZ 86001-7034, USA
[f] NASA Jet Propulsion Laboratory, 4800 Oak Grove Drive, MS 300-243, Pasadena, CA 91109, USA

ARTICLE INFO

Article history:
Received 6 December 2010
Revised 3 October 2011
Accepted 24 October 2011
Available online 6 November 2011

Keywords:
Mars, Surface
Volcanism
Geological processes

ABSTRACT

A multidisciplinary approach involving various remote sensing instruments is used to investigate Apollinaris Mons, a prominent volcano on Mars, as well as the surrounding plains for signs of prolonged hydrologic and volcanic, and possibly hydrothermal activity. The main findings include (1) evidence from laser altimetry indicating the large thickness (1.5–2 km at some locations) of the fan deposits draping the southern flank contrary to previous estimates, coupled with possible layering which point to a significant emplacement phase at Apollinaris Mons, (2) corroboration of Robinson et al. (Robinson, M.S., Mouginis-Mark, P.J., Zimbelman, J.R., Wu, S.S.C., Ablin, K.K., Howington-Kraus, A.E. [1993]. Icarus 104, 301–323) hypothesis regarding the formation of incised valleys on the western flanks by density current erosion which would indicate magma–water interaction or, alternatively, volatile-rich magmas early in the volcano's history, (3) mounds of diverse geometric shapes, many of which display summit depressions and occur among faults and fractures, possibly marking venting, (4) strong indicators on the flanks of the volcano for lahar events, and possibly, a caldera lake, (5) ubiquitous presence of impact craters displaying fluidized ejecta in both shield-forming (flank and caldera) materials and materials that surround the volcano that are indicative of water-rich target materials at the time of impact, (6) long-term complex association in time among shield-forming materials and Medusae Fossae Formation.

The findings point to a site of extensive volcanic and hydrologic activity with possibly a period of magma–water interaction and hydrothermal activity. Finally, we propose that the mound structures around Apollinaris should be prime targets for further in situ exploration and search for possible exobiological signatures.

1. Introduction

Similar to Earth, the geologic record of Mars likely includes impact-generated (Newsom, 1980; Rathbun and Squyres, 2002; Abramov and Kring, 2005) and magmatic-driven (Dohm et al., 1998, 2008; Schulze-Makuch et al., 2007) hydrothermal activity. This is deduced from the widespread occurrence of impact, volcanic, and water-related features on the surface, which are often temporally and spatially associated. Martian surfaces of different ages, for example, exhibit hydrological features such as large outflow channels (Baker and Milton, 1974), valley networks (Scott et al., 1995), gullies and debris aprons (Malin and Edgett, 2001), polygonal-patterned ground (Kargel, 2004; Levy et al., 2009; El Maarry et al., 2010), glaciers (Kargel and Strom, 1992), rock glaciers (Mahaney et al., 2007), deltas (Ori et al., 2000a; Malin and Edgett, 2003; Di Achille and Hynek, 2010), and possible water bodies ranging from lakes to oceans (Scott et al., 1995; Fairén et al., 2003; Crown et al., 2005; Di Achille et al., 2006; Wilson et al., 2007; Dohm et al., 2009a), all of which indicate that Mars had liquid water on its surface at some time during its history, perhaps for considerably lengthy periods. Associated with this diverse and extensive evidence of martian aqueous activity, are the widespread and numerous impact craters (Barlow and Bradley, 1990) and massive magmatic complexes such as Tharsis and Elysium, along with their related tectonic features (Anderson et al., 2001, 2008) in addition to other diverse evidence of volcanism (Hodges and Moore, 1994). Both water and heat energy through exogenic (e.g., impact) or endogenic (e.g., magmatic) processes often interact in space and time (e.g., Carr, 1979; Newsom, 1980; Mouginis-Mark, 1990; Crown and Greeley, 1993; Tanaka et al., 1998; Dohm et al.,

* Corresponding author. Address: Institute of Physics, University of Bern, Sidler Str. 5, 3012 Bern, Switzerland.
E-mail address: mohamed.elmaarry@space.unibe.ch (M.R. El Maarry).

0019-1035/$ - see front matter © 2011 Elsevier Inc. All rights reserved.
doi:10.1016/j.icarus.2011.10.022

2001a,b), which is expected to have produced widespread hydrothermal activity on Mars.

An example of potential martian impact-induced hydrothermal activity is Gusev Crater. Spirit, one of NASA's two Mars Exploration Rovers (MER), landed in Gusev Crater and many of its findings suggest the potential for hydrothermal alteration (e.g., Gellert et al., 2004; Schmidt et al., 2008; Yen et al., 2008; Ruff et al., 2011). Another example of recently proposed impact-induced hydrothermal activity on Mars is the impact crater Toro which is located in the northern margin of the Syrtis Major volcanic province. Toro is a 42-km-diameter and 2-km-deep complex crater, having a central peak and a central pit, both of which mark structural uplift, volatile release, and collapse. In addition, putative hydrothermal mounds are observed on and around the central uplift (Marzo et al., 2010). Analysis of spectral data in Toro impact crater shows multiple mineralogic signatures that include prehnite, chlorite, Fe-smectites, and opaline material. The observed suite of minerals is believed to be hydrothermal in origin (Fairén et al., 2010; Marzo et al., 2010), being linked to the impact crater event during the Hesperian Period. These observations are supported by geochemical simulations that indicate that such hydrothermal systems would form a suite of clay minerals in the central peaks and crater margins (Schwenzer and Kring, 2009). The large energies involved in creating impact craters can sustain hydrothermal systems for long geological periods provided that the target materials are water-enriched, as evident for Mars (e.g., Kieffer and Simonds, 1980). The estimated lifetime of impact-induced hydrothermal systems on early Mars ranges from ~70,000 years for a 30-km-diameter crater, ~400,000 years for a 180-km-diameter crater, to nearly 10 Myr for a Hellas-sized basin (Abramov and Kring, 2005).

Both impact- and magmatic-driven hydrothermal systems represent locations of exobiological interest due to the ability of such environments to sustain life on Earth (Valentino et al., 1999; Glamoclija et al., 2004; Parnell et al., 2010). As a result, many efforts have been devoted to locating optimum hydrothermal targets on Mars for exploration (e.g., Newsom, 1980; Newsom et al., 2001; Dohm et al., 2004; Schulze-Makuch et al., 2007). The work presented here is inspired by such efforts, particularly focusing on Apollinaris Patera (recently renamed to Apollinaris Mons, and as such, the newer terminology is used henceforth) which has already been identified as a site of potential magmatic-driven hydrothermal activity on Mars (Farmer, 1996; Schulze-Makuch et al., 2007). In this study, we test the hydrothermal hypothesis by investigating the entire Apollinaris Mons region and looking for key indicators of hydrothermal activity. We build upon the earlier mapping efforts found in scientific literature that focused on the volcano and its surroundings making use of the existing image databases (see online supplementary material) from the Thermal Emission Imaging System (THEMIS; Christensen et al., 2004), the narrow angle Mars Orbiter Camera (MOC; Malin et al., 1992), the Context Imager (CTX; Malin et al., 2007), and the High Resolution Imaging Science Experiment (HiRISE; McEwen et al., 2007) cameras (approximately on average, 16–40 m/pixel, 1.5–20 m/pixel, 6 m/pixel, and 25 cm/pixel, respectively), topographic data from the Mars Orbiter Laser Altimeter (MOLA; Smith et al., 2001), and spectral data from the Compact Reconnaissance Imaging Spectrometer for Mars (CRISM; Murchie et al., 2007). Our primary objective is to assess the role of Apollinaris Mons in forming an extensive hydrothermal system that could be of significant interest for future in situ exploration, and simultaneously, review and build up on the current knowledge regarding the general morphology and geology of the various geological units comprising Apollinaris Mons and its surroundings as well as its stratigraphical and chronological relation with the Medusa Fossae Formation.

2. Morphology of Apollinaris Mons

2.1. Context and literature review

Apollinaris Mons (Fig. 1) is a prominent 200 km-wide and 5 km-high shield volcano with an average slope of ~5° (Plescia, 2004). It is located near the boundary between the northern plains and southern highlands (174.4°E, 9.3°S) and approximately 200 km north of Gusev Crater, the target of investigations by the Spirit rover (Squyres et al., 2004; Arvidson et al., 2006, 2008, 2010). It contains a multi-stage caldera complex approximately 80 km in diameter. The northern and eastern flanks of the edifice are surrounded by the Medusae Fossae Formation (MFF) (Scott et al., 1993) and terminate with clear scarps. The southern flank, however, is characterized by extensive fan deposits that drape parts of the volcano from summit to base. The western flank is surrounded by large (km-sized) blocks and knobs forming a terrain similar to the chaotic terrain found elsewhere on Mars such as those that source the channels of the circum-Chryse outflow chan-

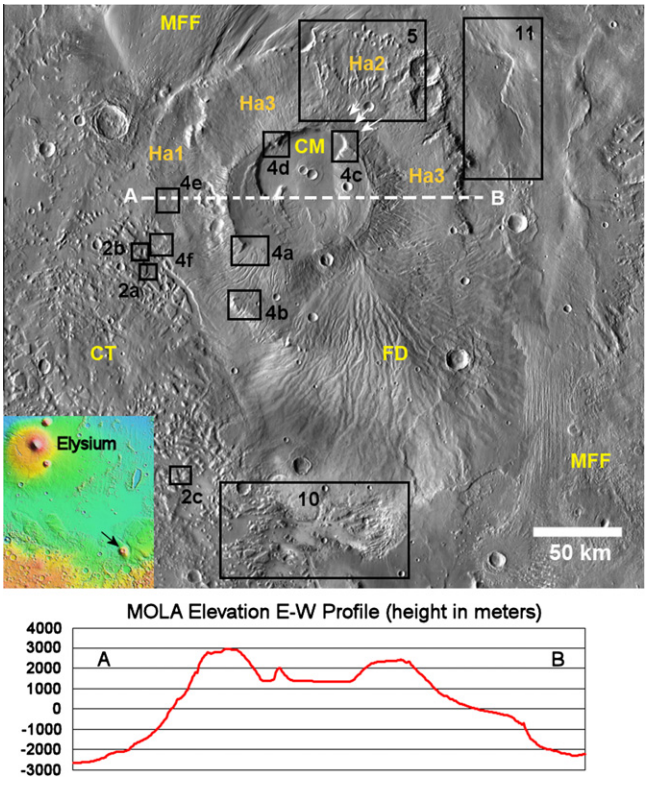

Fig. 1. (Top): Day-time IR THEMIS mosaic (100 m/pixel) of Apollinaris Mons and surrounding terrain. Apollinaris Mons occurs near the boundary that separates the northern plains from the southern highlands. Medusa Fossae Formation (MFF) partly surrounds the shield volcano to the north and east, and chaotic terrain (CT) is prevalent to the west of the volcano. The main construct is almost 200 km wide, displaying a caldera complex at its summit that is almost 80 km in diameter where the inner caldera material (CM) is affected by two impact events creating craters that are 4–5 km wide with rampart ejecta. The volcano is also notable for the extensive fan deposits (FD) that drape the southern flank and appear to originate from a small channel that dissects the southern rim. Black rectangles display the position of numerous images shown throughout the paper and the white arrows in the NE flank point to a spot suggested by Robinson and Smith (1995) to contain mineral deposits formed by fumarolic activity (see text). Other abbreviations in the figure include the geological classification of various units of the main edifice by Scott et al. (1993) from oldest to youngest which are Ha1, Ha2, and Ha3. Mosaic credit: JMARS. (Bottom): MOLA elevation profile passing through the area shown as a dashed white line in the top panel. Note the difference in steepness between the eastern flank where a notable scarp is present (right) and the western one (left) that shows various incised valleys.

nel system (e.g., Rodriguez et al., 2005). This region is characterized by mesas with heights and widths that range from 200 to 300 m and 5 to 10 km, respectively.

The orientation and shape of blocks nearest to the western flank strongly suggest that they broke off from the main edifice. The southwestern mesas occasionally display degraded and elongated geometric shapes, often paralleling the relatively large southwest–west-trending channels, and are distinctly terraced, possibly attributed to differential erosion by water and/or wind (Fig. 2a). Some mesas even show distinctive flow features (Fig. 2b). Topographic lows among the mesas are usually smooth in appearance, but are occasionally marked by small (50–100 m) pedestal or rampart craters (Fig. 2c).

Apollinaris Mons is reported to have been constructed by both pyroclastic and effusive eruptions (Robinson et al., 1993). The age of emplacement is estimated to range from the Late Noachian to the Late Hesperian Epochs based on both stratigraphic relations and impact crater statistics (Scott et al., 1993; Robinson et al., 1993; Greeley et al., 2005), or 3.8–2.9 Gyr, estimated absolute ages based on Hartmann and Neukum (2001).

The first detailed geologic mapping of Apollinaris Mons was carried out using Viking images (Robinson et al., 1993; Scott et al., 1993). Robinson et al. (1993) concluded that the volcano has two surface materials: old, easily eroded edifice material, and younger more competent fan deposits draping the southern flank. Consequently, they have proposed that large-scale explosive activity occurred during the formation of the main edifice while the fan deposits were subsequently emplaced by lavas with low eruptive rates similar to pahoehoe lavas on Earth. On the other hand, Scott et al. (1993) concluded that the initial lava flows were effusive at first forming the lower part of the volcano followed by more explosive pyroclastic events forming the upper steeper part of the edifice. At some point, depletion of the magmatic chamber led to caldera collapse, and later eruptions filled the collapsed caldera and overflowed through a small notch in the southern margin to form the fan deposits.

The Viking-era mapping investigations pointed to the Apollinaris volcano and surrounding region as a potential environment of significant magma and water interactions, and consequently, possible hydrothermal activity (Farmer, 1996). This includes possible presence of pyroclastic deposits, breaking up of parts of the volcano to form chaotic terrain, and a network of valleys along the southern margin of the above-mentioned Hesperian-aged fan deposit (Gulick and Baker, 1990; Scott et al., 1993).

Additional indicators of water enrichment at Apollinaris Mons and surrounding region include numerous valleys that dissect the caldera walls at the summit of the prominent volcano (Gulick and Baker, 1990; Farmer, 1996). A magma–water interaction hypothesis is consistent with Gamma Ray Spectrometer-based elemental information that indicates elevated hydrogen and chlorine when compared to the rest of the equatorial region of Mars (Boynton et al., 2004; Keller et al., 2006; Dohm et al., 2008). Additionally, a hypothesized ancient ocean existing during at least part of the Noachian Period and possibly extending into the Early Hesperian, may have covered approximately 1/3 of the surface of Mars (Clifford and Parker, 2001; Dohm et al., 2009a; Di Achille and Hynek, 2010), inundating the Apollinaris Mons surroundings.

Additional works include utilization of the higher-resolution image data and new observation techniques to examine its relationship with the basalts of the Gusev Crater plains (Lang

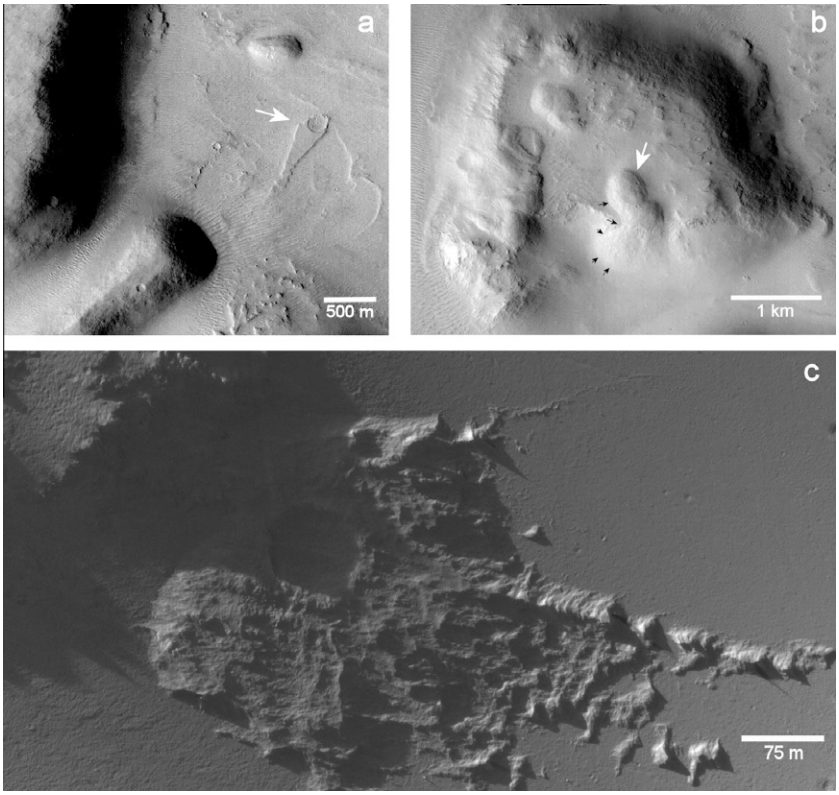

Fig. 2. High resolution images for interesting features in the chaotic terrain (CT) west of Apollinaris Mons that are discussed in the paper: (a) Small (100 m in diameter) impact crater displaying tear-drop-shaped ejecta which is indicative of either water or wind erosion, (b) possible flow features at the top of a mesa. Materials appear to originate from a point source or a fissure which is now completely buried, and extending outwards to produce a flow-like feature (arrows show the feature's boundaries) over the mesa's scarp, (c) an excellent example of a 70-m pedestal crater taken with HiRISE. The crater shows considerable erosion (probably by wind) of the ejecta deposits. Such craters are indicative of the presence of volatiles in the near surface. Image IDs: (a and b) CTX, P08_003966_1721, (c) HiRISE, PSP_009451_1675.

et al., 2010), assessment of the possible contributions of Apollinaris Mons to the MFF deposits (Kerber and Head, 2010), and study of the magnetic anomalies associated with the region (e.g., Langlais and Purucker, 2007; Hood et al., 2010).

2.2. Fan deposits

The fan deposits (FD) comprise the largest geologically distinct unit of the volcano (in surface area), starting from a distinctive breach in the southeastern part of the caldera summit and radiating downwards for almost 150 km with no obvious topographical barriers confining the deposits (Fig. 3). The fan is dissected with numerous narrow channels that form first-order tributaries in many areas with no observable distributaries (Gregg and Krysak, 2011). The morphology of the channels has been suggested to indicate formation by pyroclastic flows, lahars, or fluvial processes (Gulick and Baker, 1990; Ghail and Hutchison, 2003; Farrell and Lang, 2010; Gregg and Krysak, 2011) contrary to formation by lava flows as reported by Robinson et al. (1993). There are a number of large (>1 km) impact craters that mark the fan deposits; they display rampart ejecta and layering on the crater wall (Lang et al., 2010), hinting at a volatile-rich and layered material composing the fan.

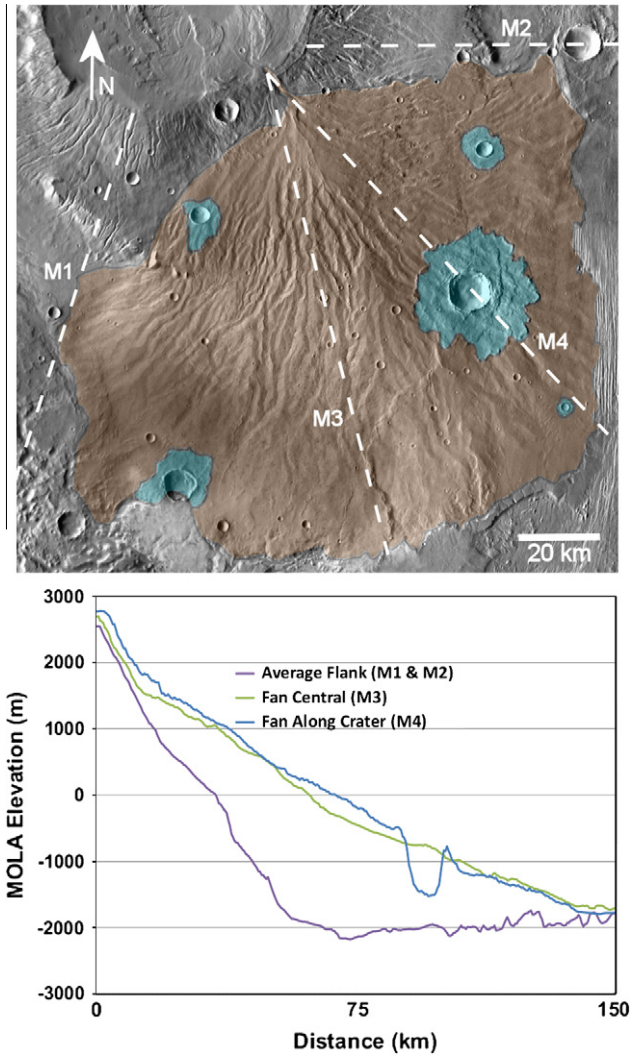

Fig. 3. (Top): Colorized mapping of the fan deposits (FD) unit along with the rampart craters overlying it and position of MOLA profiles discussed in the text overlain on daytime THEMIS-IR mosaic. The occurrence of impact craters with fluidized ejecta suggests a water-rich composition for the deposits. (Bottom): MOLA profiles shown in the top panel. The averaging of both M1 and M2 profiles allows an estimate to be made of the morphology of the volcano's flank beneath the FD. The apparent thickness of the fan deposits reaches 2 km in some locations. Note the M4 profile that indicates that the 5-km impact crater with fluidized ejecta has most likely excavated material entirely from within the FD thereby implying a fluid-rich material. (For interpretation of the references to color in this figure legend, the reader is referred to the web version of this article.)

MOLA elevation data allow us to estimate more accurately the extent and volume of the FD, as shown in Fig. 3. Considering the near-radial symmetry of the edifice, the averaging of profiles M1 and M2 should yield a reasonable estimate of the shape of the edifice underlying the FD. The MOLA data reveal that the FD are thicker than previously estimated in literature (e.g., Robinson et al., 1993), reaching a thickness of 1.5–2 km at some locations. . It should be noted that these values represent an upper limit with the assumption that the fan deposits are uniform throughout with respect to composition. Indeed, recent radar measurements of the fan deposits (El Maarry et al., 2011) do not display material heterogeneities at the resolution of the Shallow ground-penetrating radar (SHARAD; 10 m vertical resolution at ~1 km probing depth).

This data allows the estimation of an average volume of ~30,000 km^3 assuming a uniform cross-section. This value is considerably higher than recent estimates of 1000 km^3 made by Gregg and Krysak (2011), which is partly based on the FD estimate of 100–250 m generated by Robinson et al. (1993), but is markedly lower than the estimated value of 60,000 km^3 determined by Ghail and Hutchison (2003). However, these earlier estimates did not benefit from laser altimetry and in the case of the Robinson et al. investigation, only photoclinometric and shadow measurements were possible. Furthermore, the thin nature of the deposits interpreted by Robinson et al. was based primarily on an observation that the pre-existing underlying basal scarp was still evident in some parts of the eastern scarp. However, the central part of the fan deposits has an apparent thickness of ~1 km above the average elevation of the scarp, while the lowest elevation is recorded in its eastern part, only 200 m lower than the central part, making it unfeasible that the scarp would lie only 150–200 m below the fan. An alternative explanation is that the basal scarp has a higher elevation under certain parts of the fan, which is unlikely given the general uniformity of the whole main edifice. In light of this, we propose that the new values presented in this study are potentially more accurate.

The layered nature of the FD as indicated by superimposed impact craters (Lang et al., 2010) and possibly ground-penetrating radar (El Maarry et al., 2011) coupled with its estimated total volume is a strong indicator of a significant emplacement phase at Apollinaris Mons, a marker of more ancient, dynamic, and extensive magmatic-driven activity sourcing from the very prominent and seemingly isolated volcano. It is worth noting that the eastern margin of the FD is reported to overly stratigraphically one of the MFF units to the east (Lang et al., 2011) which highlights the intricate history between Apollinaris Mons and the MFF deposits. This complex relation is discussed further in a later section.

2.3. Main edifice and caldera

The main edifice is generally heavily modified by valleys, slumps, and impact craters (Robinson et al., 1993), and is characterized by steep slopes (8% on average reaching maximums of ~15% in some locations). Most of the edifice terminates in a well-defined basal scarp especially prominent along its eastern flank. As discussed already, the southern flank is covered by the fan deposits. The rest of the edifice, however, is clearly visible with the west flank displaying the steepest slopes and largest concentrations of incised valleys (Figs. 1, 4a and b), as well as multiple rock and debris slides (Fig. 4e and f), indicating a possible

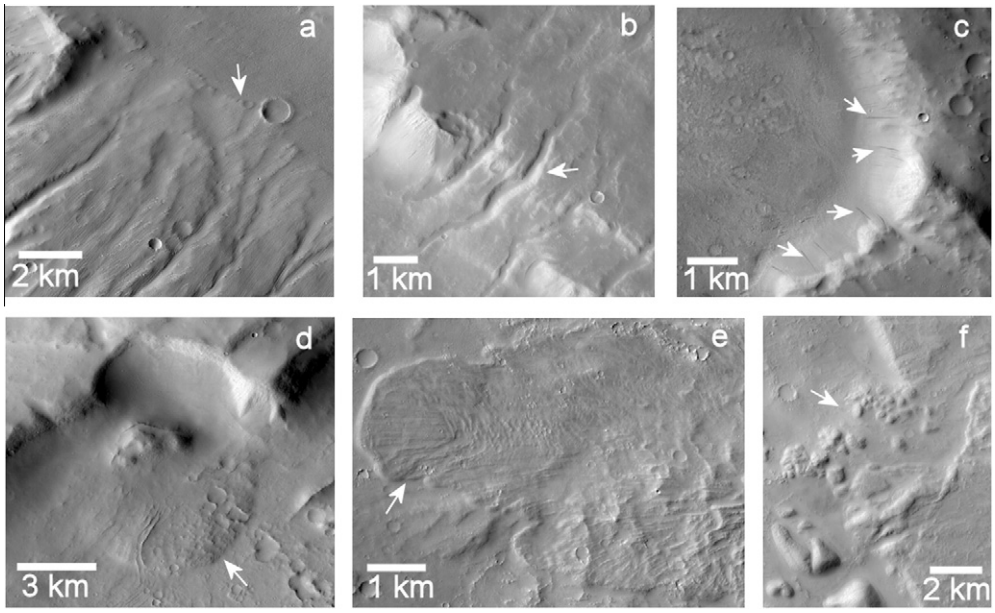

Fig. 4. CTX images of features on the flanks and inner caldera of Apollinaris Mons that are discussed in the text: (a and b) close-ups of some of the incised valleys on the volcano's west flank. Note the sharp contact between the valleys and the caldera rim (a) and the discontinuous and almost non-meandering of the valleys even over topographically rough terrains (b) which strongly suggests a density current erosion as a formation mechanism as opposed to fluvial processes, (c) dark slope streaks on the eastern caldera wall almost 1 km in length, (d) a rock- or landslide inside the caldera previously interpreted in the Viking images as an impact crater, (e and f) putative rock glaciers and rock slides at the base of the western flank, respectively which hint at the friable nature of the flank material and possible water enrichment. Image IDs: (a) B05_011653_1714, (b) B12_014132_1721, (c) P02_001988_1709, (d) P06_003544_1703, (e) P02_001843_1716, (f) P02_001843_1716.

correlation between the steep slope and presence of incised valleys. Together with the east and northwest parts, the west flank comprises the Ha3 unit as described by Scott et al. (1993) in their geological map of the region. For clarity, we have chosen to adopt the same terminology throughout this work as indicated in Fig. 1. The Ha2 unit on the north-eastern part (Fig. 5) displays a unique morphology characterized by a degraded terrain, subdued features such as impact craters, and strong indication of slumped material at the base of the edifice in contact with the MFF deposits (Figs. 5 and 6)), as well as evidence for surface runoff and/or groundwater sapping processes. The unit is greatly modified by the presence of two large (18–20 km) impact craters that could be responsible for triggering erosion of the flank material by hydrologic means to create the unit's morphology, which is particularly similar to some erosional features at the circum-Hellas shield volcanoes, Hadriaca and Tyrrhena (Greg et al., 2002 and references therein; Crown et al., 2005).

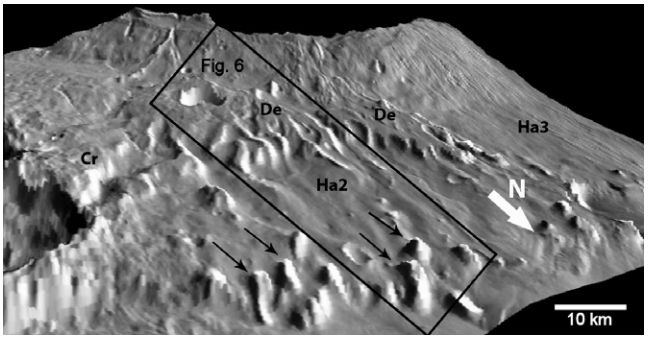

Fig. 5. Digital terrain model (vertical exaggeration: 15×) of the NE flank termed Ha2 unit in the geologic map by Scott et al. (1993). Notice the degradation of the old ejecta deposits (De) of a 5 km-sized impact craters into dendritic landforms and the large blocks (black arrows) at the base of the volcano that appear to have been mass-wasted. The erosional features may have been tectonically triggered by the 12-km crater impact (Cr). Image credit: JMARS.

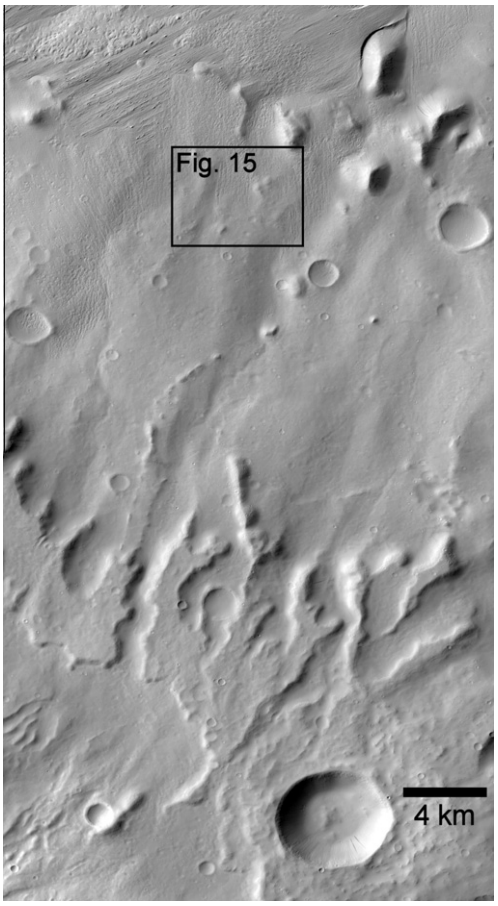

Fig. 6. CTX sub-image for the Ha2 unit deposits. The unit appears smoother than the surrounding terrain with most impact craters appearing degraded or subdued, and many valleys dissecting the unit that lack distributaries but occasionally show tributaries. Image ID: P02_001645_1726.

Finally, the caldera complex is highly indicative of multiple stages of activity with the presence of arcuate fractures, several terraces, and concentric scarps (Fig. 1; also see Crumpler et al., 1996), indicating subsidence of the caldera floor at some point. Parts of the caldera wall are friable as indicated by the rock slide at the northwest part that has formed a visible debris apron on the caldera floor (Fig. 4d). Interestingly, the eastern wall displays an array of dark slope streaks (Fig. 4c) which have been reported on Mars by several workers (e.g., Ferguson and Lucchitta, 1983; Sullivan et al., 2001; Ferris et al., 2002; Miyamoto et al., 2004; Chuang et al., 2007 and references therein). The dark streaks appear confined to this part of the caldera as well as initiating at the same height indicating some form of structural control. Proposed formational mechanisms range from debris mass wasting (Chuang et al., 2007 and references therein) to briny liquid flows (Ferris et al., 2002; Miyamoto et al., 2004).

The incised valleys on the west flank pose an important question as to their origin. Robinson et al. (1993) favored their formation through volcanic density current erosion (see Reimers and Komar, 1979) as opposed to surface runoff and sapping (Gulick and Baker, 1990). This interpretation was based on the criteria that density currents are expected to erode near the summit and are generally insensitive to local topographic variations (Reimers and Komar, 1979) as opposed to runoff valleys that alternatively would be expected to form tributaries and follow the local topography. High-resolution CTX images allow the testing of this original hypothesis. Indeed, the valleys appear discontinuous, lacking tributaries, and appear to terminate abruptly. Additionally, many of the valleys are covered by eroded ridges and solidified dune-like material that was additionally proposed by Reimers and Komar (1979) to indicate erosion by density currents. Finally, almost all the valleys on the western flank appear to initiate at the outermost rim of the caldera rather sharply as proposed by Robinson et al. (1993), although this may also suggest that the caldera collapse occurred subsequent to the development of the channels, thereby truncating them (Crumpler et al., 1996). On the basis of these observations, we concur that these valleys are likely to have formed through density current erosion as initially proposed by Robinson et al. (1993). The presence of the valleys almost entirely associated with the outer caldera rim indicates that the earliest eruptions were highly explosive and involved interaction with water at the surface or volatile-rich magmas.

3. Features associated with Apollinaris Mons

3.1. Tectonic features

Apollinaris Mons is an isolated major vent structure. A regional digital paleotectonic mapping investigation highlights primary and secondary centers of magmatic- and impact-induced driven tectonic activity in the eastern hemisphere, including Elysium, Hadriaca/Tyrrhena, Isidis–Syrtis, and Arabia Terra, but not in the Apollinaris and surrounding region (Anderson et al., 2008). In addition to an identified northwest-trending prominent structural zone of crustal/lithospheric weakness near the northeastern flank of the shield volcano (Dohm et al., 2007), there are dominantly northwest- and northeast-trending structures (Fig. 7) that comprise lineaments interpreted to be faults, fractures, or scarps formed by tectonism as well as wrinkle ridges which are indicative of subterranean thrust faulting (usually in volcanic flows). As on Earth, tectonic structures can control the migration of fluids such as magma, water, and other volatiles, as well as heat energy in the subsurface, influencing hydrogeologic and volcanic activity such as observed within the Thaumasia region on Mars (Dohm et al., 1998, 2001b; Tanaka et al., 1998), and terrestrially, the San Francisco and Mormon volcanic fields of northern Arizona near the Grand Canyon (Dohm, 1995; Holm, 2001), the Chilean Atacama Desert (Warren-Rhodes et al., 2007; Hock et al., 2007), and Solfatara Crater, Italy (Chioni et al., 1984).

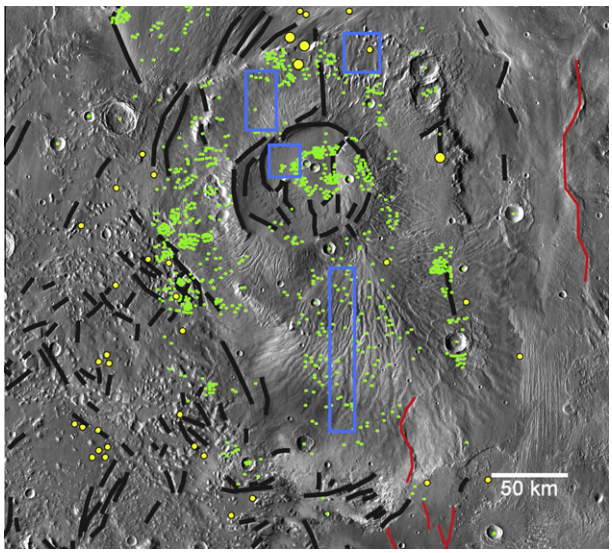

Fig. 7. Day-time IR THEMIS mosaic (100 m/pixel) of Apollinaris Mons and surrounding terrain showing distributions of isolated mounds (small yellow circles) and clustered ones (large yellow circles), impact craters with associated fluidized ejecta (green) which were identified using CTX images, thereby explaining the apparent lack of craters in the chaotic terrain where CTX images are not available (see online supplementary material), lineaments interpreted to be faults, fractures, and scarps formed by tectonism, collapse, and/or erosion (black lines), wrinkle ridges (red lines), and areas where crater counting was performed (blue boxes). Mosaic credit: JMARS.

3.2. Mounds

Mounds occur on the flanks of Apollinaris Mons and its surroundings. Several display distinct central depressions (Fig. 8). They generally form two distinct groups: large (0.2–3 km in diameter) isolated structures mainly situated in the chaotic terrain and smaller (100 m-sized) mounds forming distinctive clusters situated on the northern and eastern flanks of the volcano and in the MFF deposits located to the north (Fig. 7). Some of the mounds are found associated with tectonic features which may indicate some basement-control.

Furthermore, the mounds are characterized, in general, by relatively higher brightness temperatures with respect to their surroundings in night-time THEMIS images (Fig. 9). This likely indicates that the mound-forming materials have higher thermal inertia values than those of the surrounding materials. However, quantitative measurements of thermal inertia derived from the THEMIS images (Fergason et al., 2006) for some of the mounds yield low thermal inertia values in the range of 90–215 J m^{-2} K^{-1} $s^{-1/2}$ (Table 1). Such values correspond to a dusty component or indurated fine sand at best covering at least the top 2 cm of the surface.

Mounds and pitted cones are a common feature on the martian surface, especially prevalent in the Vastitas Borealis Formation of the northern plains (Tanaka et al., 2005). Tharsis-derived floods are proposed to have contributed to the inundation of the northern plains to form large water bodies ranging in size from lakes to oceans (Baker et al., 1991; Fairén et al., 2003; Dohm et al., 2009a). These flooding events, which resulted in the dissection and removal of kilometers-deep crustal materials in the cratered highlands, are suspected to have contributed to the emplacement

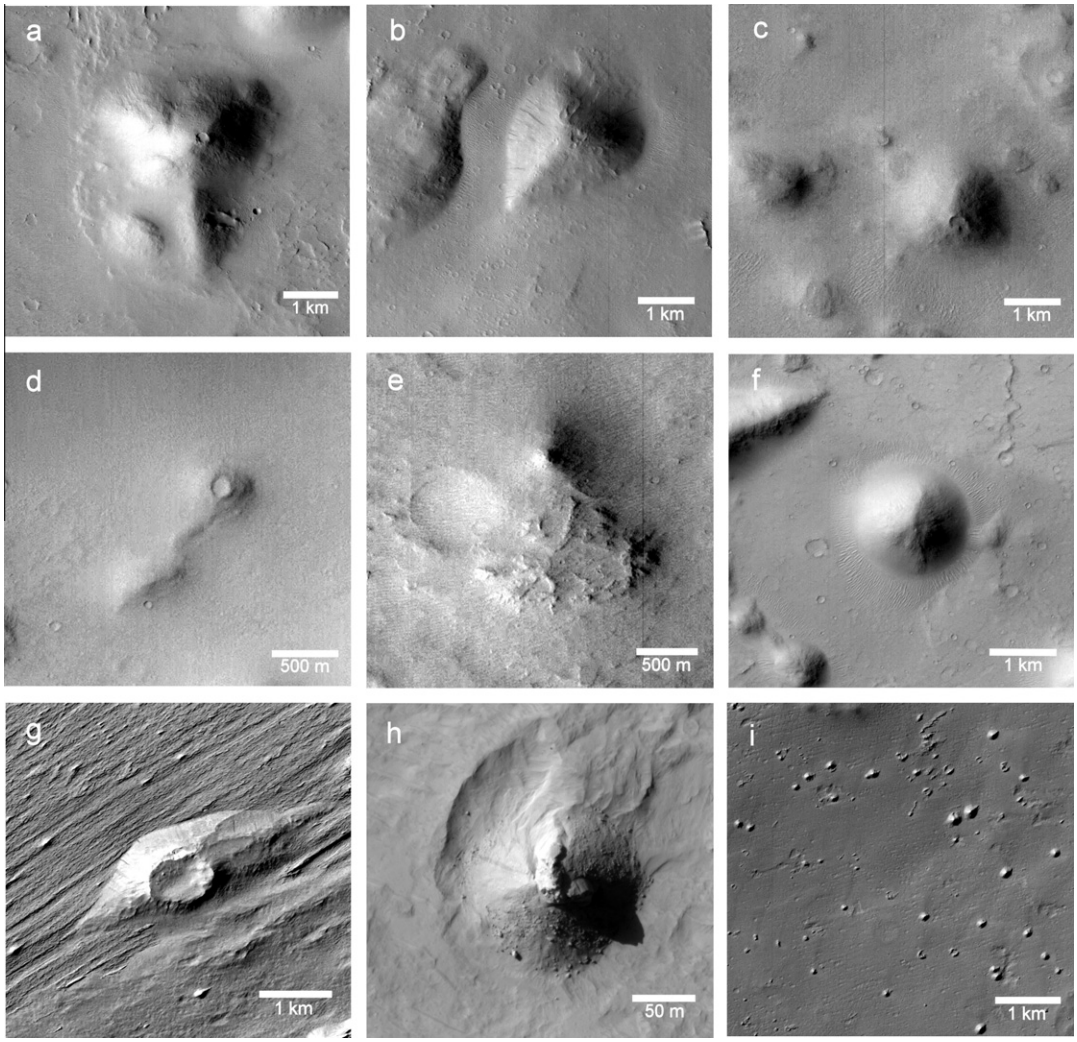

Fig. 8. Examples of mounds observed at Apollinaris. The mounds range in size from 0.1 to ~3 km in diameter and have variable shapes. Shadow analysis reveals a variation in width to height ratio, though quantitative information cannot be determined. The mounds form two distinct groups: Large 0.2–3 km-sized isolated structures that are pitted in some locations (d, e, and g), and clusters of smaller (100 m-sized) cone-like structures located on the northern flank of the main edifice and close to the MFF (i). Some appear to be spatially associated with faults and fractures, possibly indicting basement structural control. The variable morphologies can be indicative of different formation mechanisms. Image IDs: (a, b and e): P08_003966_1721, (c and d): P13_006234_1664, (f): P15_007091_1668, (g): P16_007236_1754, (h): PSP_007671_1695, and (i): P18_007882_1703. All images are CTX images except for (h) which is an image taken by HiRISE for a 100 m-wide mound located on the boundary which separates the fan deposits and the wind-etched MFF materials in the east. Materials appear to be pyroclastic in origin.

of hyperbyssal flows and related constructional landforms such as mud volcanoes (e.g., Ori et al., 2000b; Skinner and Tanaka, 2007; Allen and Oehler, 2008) and associated piping structures (Mahaney et al., 2004). While volatile-release features may aptly explain many of the constructional features, cinder cones (Scott et al., 1995), cryptodomes (Rampey et al., 2007; Farrand et al., 2011), pseudocraters (aka rootless cones) related to the interaction of ground ice or water with volcanic flows (Carr, 1986), pingos and ice-cored ridges (Lucchitta, 1981; Rossbacher and Judson, 1981), or mounds formed by the disintegration of stagnant ice covers (Grizzaffi and Schultz, 1989), are some of the previously proposed mechanisms that cannot be ruled out as possible explanations for the formation of some of the conical hills. The challenge of assigning a unique formation mechanism to these mounds is further explored in Section 7.

3.3. Channels and valley systems

Apollinaris Mons displays on its flanks a variable suite of valleys and putative channels as already described by previous workers (e.g., Gulick and Baker, 1990; Scott et al., 1993; Farmer, 1996) with the most significant being the narrow incised channels and valley networks on the western and northeast flanks respectively (Gulick and Baker, 1990) in addition to the valleys which dissect the fan deposits (Gulick and Baker, 1990; Gregg and Krysak, 2011). In addition, one of the most prominent features around Apollinaris Mons is the large valley system at the distal margin of the southern flank, which extends to the southwest, eventually transitioning into the chaotic terrain where the system no longer can be mapped. The valley system has widths and depths reaching 20 km and 500 m, respectively (Fig. 10), and appears to spread out from a single source region at the southern margin of the fan deposits and then extends westward for almost 120 km. Its morphology is comparable to the outflow channels surrounding Chryse Planitia, although being orders of magnitude smaller. On Earth, such terraced promontories often record water-related modification (and/or wind activity) including dissection during flooding, lake- and ocean-related wave cutting, and thawing of ice-enriched materials in periglacial environments, which result in retrogressive debris flows often marking significant environmental change such as

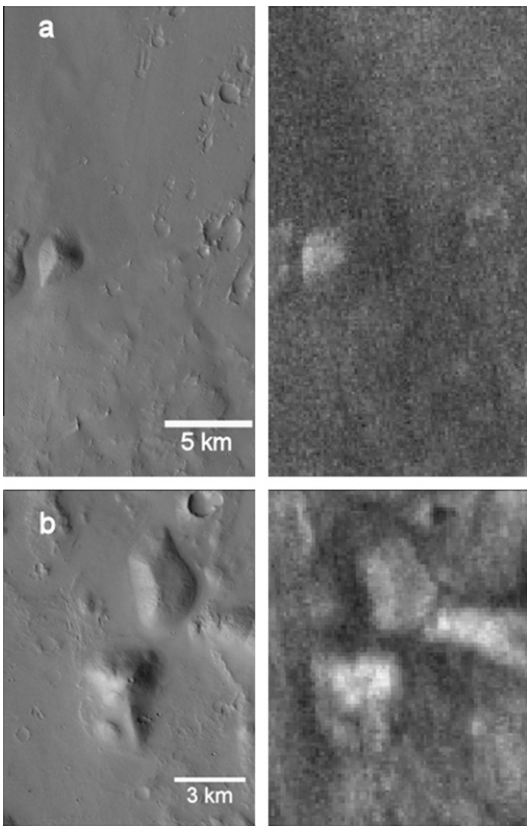

Fig. 9. Night-time infra-red data for some of the Apollinaris mounds (locations: 7.39°S, 172.36°E, and 11.91°S, 173.82°E, respectively). Mounds appear to have a higher temperature than the surrounding terrain thereby implying a higher thermal inertia. Nevertheless, quantitative estimates reveal low absolute thermal inertia values (see Table 1) corresponding to fine sand material or variably indurated dust covering the upper 2–4 cm of the surface. Images IDs: THEMIS-IR (a) I31987009 and (b) I172000013.

Table 1
Derived thermal inertia values for a number of the mounds found around Apollinaris Mons. Generally, thermal inertia values are low indicating fine-grained sand or variably-indurated dusty material. Images used for derivation of thermal inertia are THEMIS-IR images I31987009 for the first two mounds and I172000013 for the third one.

Latitude	Longitude	Thermal inertia ($J\ m^{-2}\ K^{-1}\ s^{-1/2}$)
7.39S	172.36E	112 ± 22
8.94S	172.62E	187 ± 17
11.91S	173.82E	153 ± 13

highlighted at Old Crow Basin located in Vuntut National Park, Canada (Fulton, 1989; Mathews, 1990). Parts of the fan deposits appear to have been separated from the volcano related to the formation of the channel system (Fig. 10).

Another feature, which marks water activity around the shield volcano, is a valley system dissecting the MFF deposits east of the main edifice (Fig. 11). Scott et al. (1993) mapped and characterized this system using Viking data as "material deposited by flowing water surrounding ridges that are eroded remnants of the MFF" and assigned it an Amazonian age. Close inspection using CTX images supports this hypothesis and allows us to further track the extent and source of the valley system (Fig. 11). The system, which has a length nearing 90 km, appears to source from a ~40-m-deep depression (Fig. 12), extending northwards with an average slope of 0.5% (i.e. decreasing by 5 m in elevation per km). Narrow (~100 m wide) valleys (Fig. 12) radiate from the depression and coalesce to form the wider (~1 km wide) part of the valley system that appears to empty into another depression located northeast of Apollinaris. In addition, the main valley displays features that indicate a fluvial origin such as meandering, braiding, and streamlined structures (Fig. 13). The overall morphological characteristics of the valley system which include presence of first order tributaries, low drainage density, initiation from fractured terrain, and tectonic or structural control (Fig. 7) are strongly indicative of a groundwater-fed sapping system (Gulick, 2001).

There are various driving forces that could initiate this channel system, one of which is a hydrothermal system formed by magmatic intrusions from Apollinaris Mons. Previous works have discussed the possible role of magmatic-driven hydrothermal systems in forming fluvial channels on Mars due to the apparent spatial and temporal correlation of fluvial erosion with volcanic activity (e.g., Gulick and Baker, 1989, 1990; Tanaka et al., 1998) in addition to numerical simulations supporting this hypothesis (Gulick, 1998). Other possibilities include tectonic instabilities caused by seismic activity related to a system of faults and/or the formation of a 12-km-wide impact crater (10 km and 20 km to the west, respectively). The impact crater event could have triggered reactivation of the basement structures, thermal-induced flooding, and dissection of the MFF deposits. Alternatively, the valley could have been carved by volcanic processes. Indeed, fluvial and volcanic channels can display similar characteristics such as sinuosity, braiding, and terracing (Leverington, 2004; Bleacher et al., 2010). However, we favor a fluvial origin, triggered by either magmatic intrusions or seismic activity, based on the presence of the abovementioned features, which are more common among fluvial channels than volcanic ones, in addition to the absence of compelling evidence for volcanism such as the presence of a topographic "cap" in the source region of the valley or any visible rootless cones (pseudocraters) along the valley (Bleacher et al., 2010).

3.4. Craters with fluidized ejecta

Many impact craters on Mars display layered ejecta deposits (Barlow et al., 2000) that appear fluidized. These observations were made as early as the Mariner 9 and Viking missions (e.g., McCauley, 1973; Carr et al., 1977; Allen, 1979; Mouginis-Mark, 1979, 1987). Depending on morphology, these ejecta were historically given different names such as pedestal, rampart, lobate, and pancake. However, the current general consensus is to use the term 'Layered Ejecta Deposits' (LED) for craters with rampart, lobate, and pancake shaped ejecta, while the term 'pedestal' is conserved for layered ejecta patterns that have undergone substantial erosion, resulting in the crater and ejecta being perched above the surrounding terrain (Barlow et al., 2000). While eolian activity has been suggested to be responsible for the modification of these ejecta deposits (McCauley, 1973; Arvidson et al., 1976), it is generally accepted that LED craters are evidence of impacts into ice- or liquid water-enriched target materials (e.g., Carr et al., 1977; Mouginis-Mark, 1979; Barlow et al., 2001; Barlow, 2004; Oberbeck, 2009).

We have mapped LED impact craters using the CTX data (resolution ~6 m /pixel), as it provides sufficient resolution with the greatest spatial coverage. The image resolution facilitates the detection of impact craters with LED morphology down to ~20 m in diameter (Fig. 16), while the spatial coverage of the CTX images allowed for the investigation of the entire volcanic edifice and some of its surroundings (see Fig. 1). The distribution of impact craters with LED morphology (Fig. 14) shows their prevalence in the region, with a significant amount of these craters being pedestals, while the rest being single layered ramparts with few exceptions showing multilayered ejecta (Barlow et al., 2000). The nature

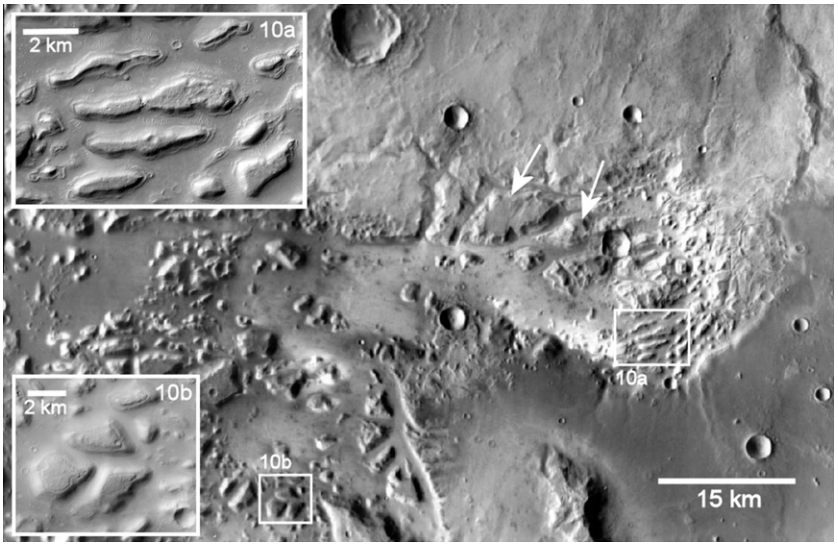

Fig. 10. Day-time IR THEMIS mosaic for the large valley system south of Apollinaris Mons resembling the outflow channels in the circum-Chryse region. The valley system is a wide depression reaching 20 km wide at some areas and 500 m deep, extending westward for almost 120 km (image credit: JMARS). Arrows point to parts of the fan deposits that appear to have been separated from the volcano related to the formation of the channel system. Inbox: Several large blocks situated in the valley show streamlined features and possible terracing. Image IDs: (10a): CTX P15_007091_1668 and (10b): CTX P18_007882_1703.

of the ejecta deposits of small (<50 m) impact craters, however, is difficult to determine.

To summarize, this investigation points to volatile enrichment at and surrounding the shield volcano for at least part of its history, including the caldera complex, the shield-forming materials, and the surrounding materials including the MFF (Fig. 7). In fact, two medium-sized impact craters are located in the central part of the caldera, which have diameters and depths of 4.8 and 6 km and 100 m and 400 m, respectively. This hints at volatile enrichment of the caldera floor materials at the time of impact crater formation that most likely post-dates Apollinaris Mons's complex volcanic activity.

4. Chronology

Crater counts for various units at Apollinaris Mons have been carried out by numerous workers (Scott et al., 1993; Robinson et al., 1993; Greeley et al., 2005; Gregg and Krysak, 2011) rendering an age of Late Noachian to Early Hesperian and an estimated absolute age of 3.8–2.9 Gyr, based on Hartmann and Neukum (2001). However, almost all these crater counts have taken place using cumulative densities of impact craters larger than 1 km. In this work, CTX images were used to produce crater counts using larger cumulative densities that include impact craters down to 250 m in diameter for different geological units at Apollinaris Mons (from oldest to youngest in previously reported ages and matching Scott et al., terminology; Fig. 1): Ha2 (North East flank), Ha3 (West and North West flanks), and Ha4 (inner caldera and fan deposits,). The crater count was carried out by measuring the cumulative density of craters larger than 500 m and 250 m for these units. We have avoided counting smaller craters in order to minimize the contribution of secondary craters to the overall population. Our crater counts were then incorporated into the free software Craterstats2 (Michael and Neukum, 2010) to derive absolute ages using the chronology function of Hartmann and Neukum (2001), and production function from Ivanov (2001). Our results are summarized in Table 2. Our results for the main edifice, caldera, and fan deposits agree well with earlier reported ages for Apollinaris Mons, albeit slightly younger, ranging from 3 to 3.4 Ga. The only exception occurs at the Ha2 unit which is markedly younger (~2 Ga) which could imply a recent resurfacing event. However, the crater population may have been influenced by two relatively large impact events (see Figs. 1 and 16) in addition to other processes that are discussed later in the paper. Similarly, the older age estimate for the inner caldera (~3.4 Ga) could mark a deviation due to the presence of many secondary craters caused by the two large impacts into the caldera.

5. Stratigraphy: relation to Medusae Fossae Formation

The Medusae Fossae Formation (MFF) is an enigmatic deposit located along the highland–lowland boundary of Mars near the equator, stretching between 170 and 240°E to the west and south of the Tharsis and Elysium volcanic provinces, respectively, and bordering the northern and eastern flanks of Apollinaris Mons. It has been mapped as one of the youngest deposits on Mars, relative-age dated as Amazonian (Scott and Tanaka, 1986). However, recent works point to an earlier age of formation for some of the materials, dating as far back as the Early Hesperian (Kerber and Head, 2010). The geologic formation is divided into seven separate units (Scott and Tanaka, 1982). Kerber and Head (2010) investigated the contact between the MFF unit north of Apollinaris and the main edifice (Figs. 6 and 15) and concluded that a part of the Apollinaris volcanic material (reworked or slumped Ha2 unit in this study) is overlying MFF deposits citing this as partial evidence for a more ancient emplacement age. We have similarly investigated the relation between the northern flank of the edifice and the MFF materials in the north (Amm unit in the USGS geological map of Scott et al. (1993); Fig. 16). The MFF can be divided into at least three separate units that show distinct vertical separation and differences in morphology (Figs. 16 and 17). All units comprise mounds and degraded craters. Unit MFF3 (Figs. 16 and 17) displays yardangs, which are characteristic of MFF deposits, and overlies unit MFF2, which in turn overlies unit MFF1. Units MFF2 and MFF3, in particular, show extensive degradation with almost complete removal at some locations (Fig. 17).

Other interesting relations arise to the northwest (unit Ha3, northwest flank; Fig. 18) and northeast (Ha2 unit, Fig. 19), respectively, where it appears that relatively late-stage emplacement phases have draped materials over the older edifice scarp and parts

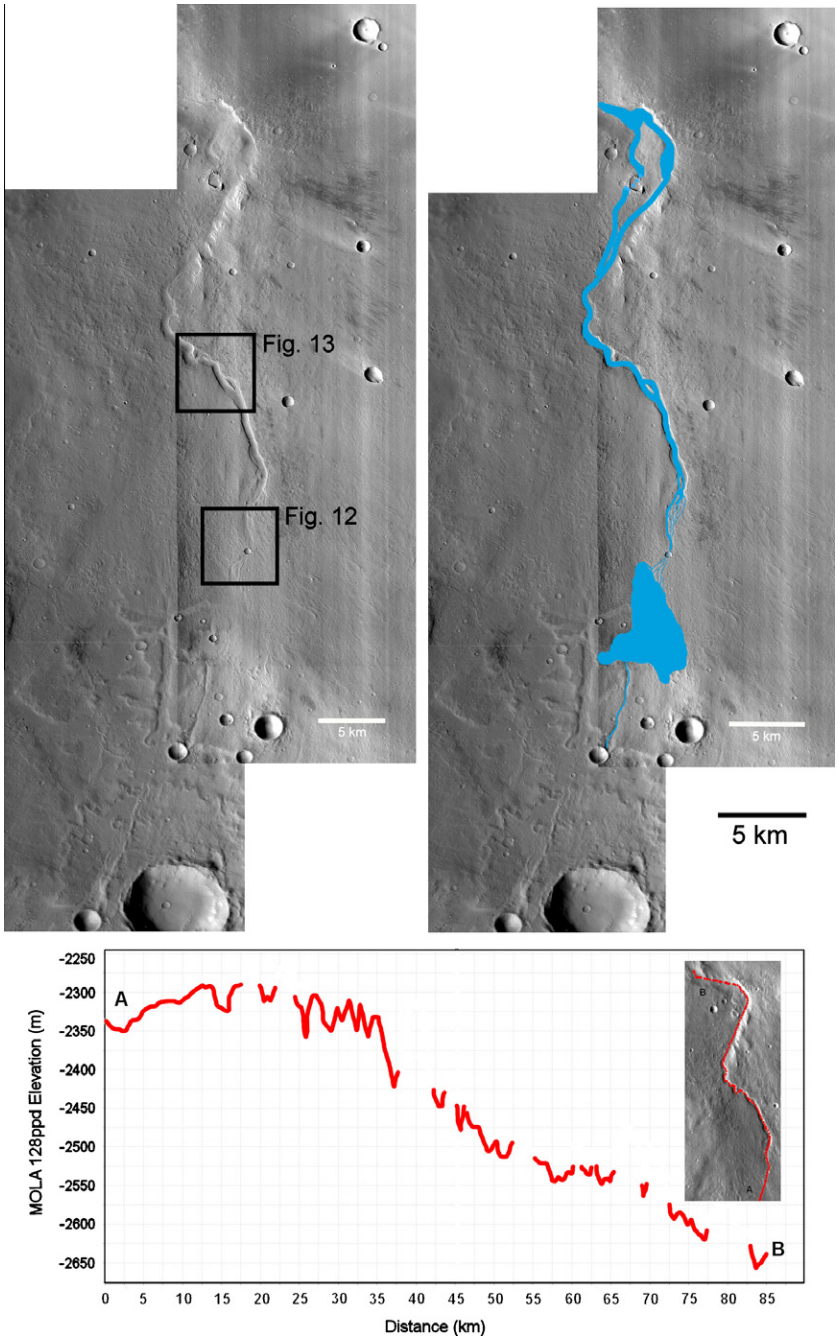

Fig. 11. (Top): CTX mosaic of the putative fluvial channel that occurs east of Apollinaris Mons. High-resolution data facilitate the tracing of this channel and its possible source (left) and highlight of the putative channel system which extends more than 90 km in length (right). Such a system may have originated through magmatic-/impact-driven hydrothermal activity or tectonic instability. The overall morphology of the valley system is strongly indicative of a groundwater-fed sapping channel system (see text). Image IDs: B09_013288_1724, and P12_005535_1732. (Bottom): MOLA profile of the channel system, including the putative source region that can be seen at point "A" in the profile. The total average slope is ~0.5%. The apparent missing points have been manually removed, as they show abnormal spikes as a result of the MOLA resolution limitations and errors arising from the manual aligning of the profile to coincide with the valley floor.

of the MFF units. The northeast area in particular, displays a very sharp boundary between the MFF1 and the MFF3 units (Fig. 19, inbox A) that could indicate an intense period of differential erosion. Moreover, it appears that reworked or slumped material of the Ha2 unit has extended away from the flank to overly the MFF deposits. This relation can be clearly seen through the material's embayment of a small impact crater on the MFF1 deposits (Fig. 19, inbox B). On the basis of these relations we interpret that differential erosion has removed an old deposit (possibly MFF2) overlying the MFF1 creating the unconformity with the MFF3 unit. This was followed by the deposition of the reworked or slumped Ha2 material (possibly through mass-wasting processes) over the MFF1 deposits.

The results of our investigation are mostly consistent with Kerber and Head (2010) in that: (1) the earliest emplacement phase of MFF deposits is earlier than previously recognized from Viking-based geologic investigations (e.g., Scott and Tanaka, 1982, 1986), (2) MFF included multiple stages of development (i.e., at least three MFF units north of Apollinaris based on this investigation), (3) the MFF deposits are friable and thus impact craters are readily eroded, altering the crater retention ages (i.e.,

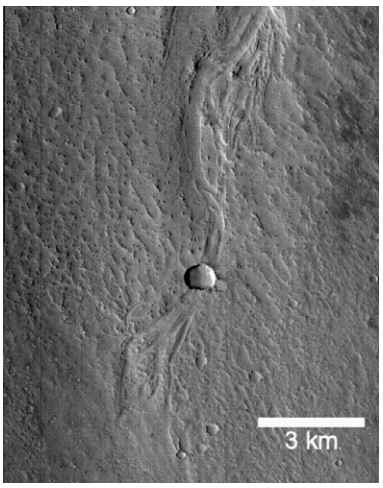

Fig. 12. CTX image displaying evidence of small branching channels that appear to source from an ancient lake that coalesced into the larger channel, consistent with Viking-based observations (Scott et al., 1993). The channels have been modified by the impact crater event. Image ID: P12_005535_1732.

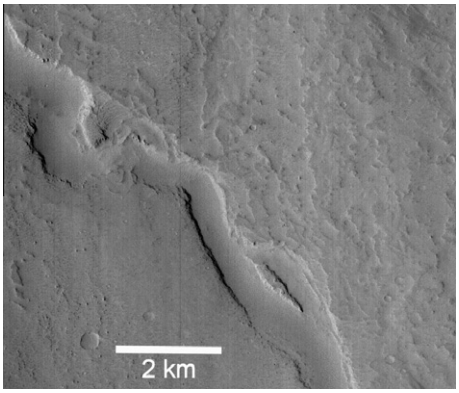

Fig. 13. CTX image showing the channel system with typical fluvial signatures such braiding, streamlined features, and meandering. Image ID: P12_005535_1732.

exhibiting an apparent younger relative age), (4) Apollinaris Mons-forming materials intermingle stratigraphically with the MFF deposits, and (5) the spatial and temporal relations among the Apollinaris materials and the MFF deposits point to Apollinaris Mons as a candidate source for at least some of the MFF deposits. It can be concluded that, similar to the MFF deposits resulting from various stages of emplacement spanning the Early Hesperian Epoch through the Late Amazonian Epoch, the fact that Apollinaris Mons has recorded events that are younger than some of these friable deposits attests to its long-term volcanic activity.

6. Mineralogy

Distinctive mineralogical signatures are arguably the most direct evidence for aquatic or hydrothermal activity. Magmatic-driven hydrothermal systems are expected to form a rich suite of minerals. As a result, an effort was made to locate mineral signatures that could be indicative of hydrothermal alteration such as clay minerals, zeolites, serpentines, sulfates, carbonates, and silica-rich deposits using data from the Compact Reconnaissance Imaging Spectrometer for Mars (CRISM; Murchie et al., 2007). CRISM is a hyperspectral imager that measures reflected radiation in the visible and near infrared (VNIR) from the surface of Mars, providing the ability to recognize both primary (e.g., olivines and pyroxenes) and secondary minerals (e.g., clay minerals). The spatial resolution of the instrument in its full-resolution configuration is ~15–19 m/pixel with 544 spectral channels and with a footprint ~14 km across.

Nine CRISM observations at different spatial resolution are currently available for the region, sampling part of the caldera and the western flank of the volcanic edifice. These observations were converted to apparent I/F (the ratio of reflected to incident sunlight), then divided by the cosine of the incidence angle to correct for the illumination geometry (Murchie et al., 2007, 2009). The atmospheric contribution was removed using an improved volcano-scan correction proposed by McGuire et al. (2009). A de-spiking and de-striping algorithm (Parente, 2008) was applied to improve the overall quality of the observation by removing artifacts. Evaluation of the CRISM data used the spectral parameters of Pelkey et al. (2007). We investigated a variety of the parameters, including those associated with hydrated and/or hydroxylated silicates, sulfates, and carbonates. Each parameter map was visually evaluated using one, or more, threshold value(s) in search for a spatially coherent pattern that potentially suggests positive identification. However, no coherent patterns were found in the eight observations considered.

A visual inspection has been carried out for each observation revealing the absence of obvious absorption bands that might have helped to assess the mineralogy of Apollinaris Mons. The spectra appear featureless across the entire structure, from the caldera to the base of the flank sampled by the CRISM observations (a typical spectrum is shown in Fig. 20). The slight positive slope in the spectral range 1.0–2.5 μm could be suggestive of iron oxides (e.g., hematite α-Fe_2O_3) and the reduced spectral contrast is consistent with the presence of fine particles (e.g., Hapke, 1981; Mustard and Hays, 1997) that cover the surface, probably masking the underlying composition.

It should be noted that Robinson and Smith (1995) interpreted a high albedo feature in the Viking images located near the caldera rim on the NE flank (Fig. 1) to be a mineral deposit formed by past fumarolic activity. Close inspection of that region in visual CTX and THEMIS infrared images doesn't show this albedo feature at all which would imply that this feature was either an artifact in the Viking images or a seasonal snow patch. Unfortunately, no CRISM data (see online supplementary material) is available to further investigate it.

7. Discussion

Schulze-Makuch et al. (2007) made use of the recent improvements in data quality (i.e., Mars Global Surveyor and Mars Odyssey) to observe distinct geologic, paleohydrologic, paleotectonic, topographic, geophysical, spectral, and elemental signatures on the surface of Mars in search of sites of potential hydrothermal activity. In doing so, they proposed a set of criteria that a certain location should display in order to be deemed a location with high hydrothermal activity potential. These criteria include: (1) evidence of action of liquid water through erosion; (2) evidence of volcanic constructs and/or lava flows; (3) evidence for a center of magmatic-driven tectonism; (4) topographical depressions hypothesized to be the result of structurally controlled collapse and/or rifting; (5) evidence for impact events in ice-rich regions; (6) presence of minerals that usually have a hydrothermal origin or that are indicative of hydrothermal alteration; and (7) geological similarity to hydrothermal analog environments on Earth. It is worth considering that not all of these criteria bear the same weight. In addition, it is feasible that an area would display one or some of these criteria without being hydrothermally active.

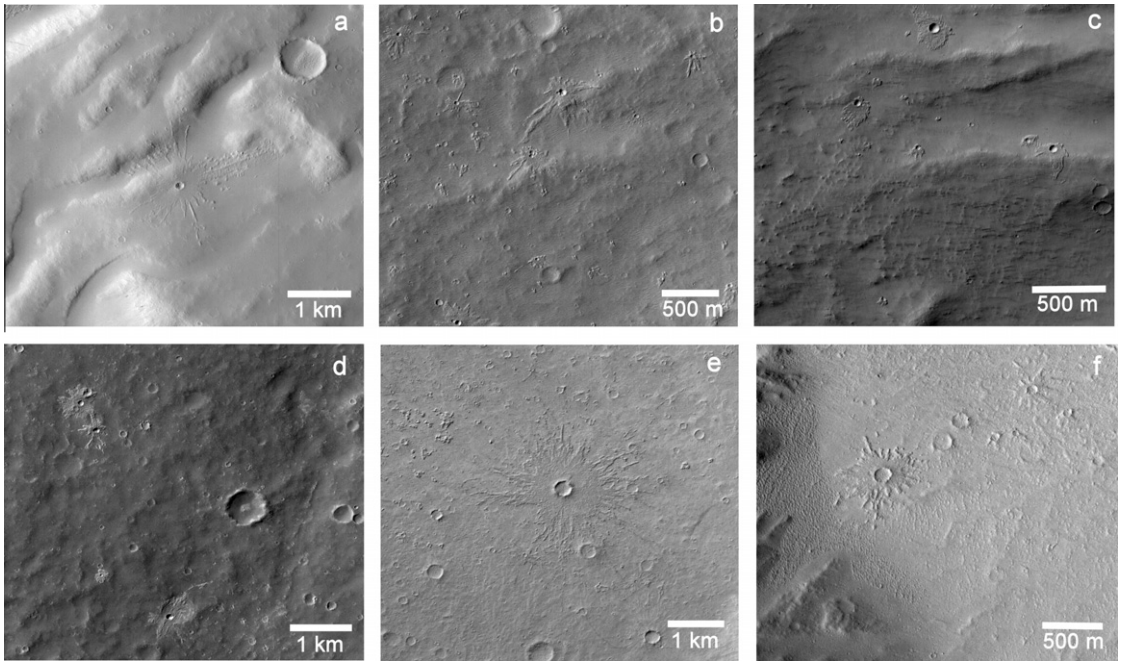

Fig. 14. Examples of small (20–200 m-wide diameters) single layered ejecta (SLE) craters at Apollinaris Mons. Most craters are either rampart or pedestal. The distribution of these craters is widespread across the volcano as they are located on the main edifice (a, b and c), the fan deposits (d), and even in the caldera complex (e and f). Image IDs: (a): B05_011653_1714, (b): P02_001843_1716, (c): P22_009596_1706, (d and e): P18_007882_1703, and (f): P06_003544_1703.

Table 2
Crater count statistics for four different units in Apollinaris Mons which are highlighted in Fig. 7. Ncum(250) and Ncum(500) represent the cumulative number of craters larger than 250 m and 500 m, respectively. D250 and D500 represent the cumulative number density of craters larger than 250 m and 500 m, respectively. The associated sigma (σ) errors are similarly shown. Absolute age computations were carried out using the free software craterstats2 in the manner described by Michael and Neukum (2010). Production function of Ivanov (2001) and chronology function of Hartmann and Neukum (2001) are used for the absolute age estimates. No resurface correction is applied. Ages are given in Ga. Images used for the crater counts are P06_003544_1703 (inner caldera; IC), B01_010163_1712 (flank material Ha3; FM), P18_007882_1703 (fan deposits; FD), and P02_001645_1726 (flank material Ha2; Ha2). Note the younger age of the Ha2 which could imply a more recent resurfacing event. Similarly, the older age estimate for the inner caldera could mark a deviation due to the unintentional incorporation of secondary craters caused by the two large impacts into the caldera.

Unit	Area	Ncum(500)	Ncum(250)	D500	σ(D500)	D250	σ(D250)	Age
IC	364	19	98	0.052	0.012	0.260	0.027	$3.35^{+0.05}_{-0.08}$
FM	733	39	123	0.053	0.008	0.167	0.015	$3.10^{+0.12}_{-0.19}$
FD	2581	130	476	0.050	0.004	0.184	0.008	$3.14^{+0.06}_{-0.08}$
Ha2	372	12	43	0.032	0.009	0.115	0.017	$2.10^{+0.32}_{-0.32}$

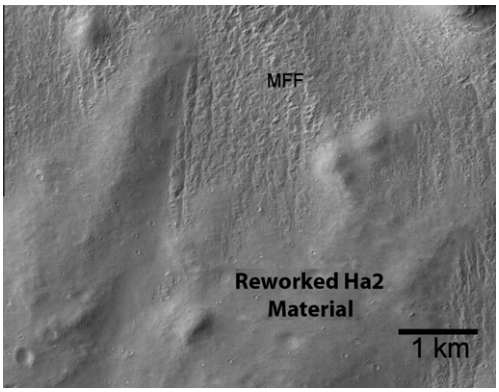

Fig. 15. Close up of the relation between the reworked Ha2 material (identified later in the text as possible lahar material) and northern deposits interpreted as MFF deposits. The MFF deposits clearly underlie the flank material. Image ID: P02_001645_1726.

However, the collective presence of all or most of these criteria would on the other hand create a strong case for hydrothermal activity.

In this work, we chose to summarize these criteria into three conditions that need to be met: (1) evidence (be it geological, geomorphological, or mineralogical) for magmatic activity; (2) evidence for water enrichment and hydrologic activity; and (3) evidence for magma–water interaction. This simplification highlights the main conditions needed for a hydrothermal system to occur: a heat source, abundance of water in any state and a suitable environment or conduit for these two to interact and create a system of convective energy loss (see Pirajno, 2009).

The collective investigation presented in the previous sections points to magmatic, water enrichment and hydrologic activity at and in the vicinity of Apollinaris Mons with a high possibility for magma–water interaction. However, the mantling of the region with fine dust makes it difficult at the time to validate the geomorphological evidence with mineralogical signatures that can be indicative of magma water interaction, and consequently, hydrothermal activity. Regardless, the strong evidence for a rich hydrologic history and prolonged volcanic activity makes it highly feasible that both processes (volcanic and hydrologic) interacted at a certain period of Apollinaris Mons' lifetime rendering this region a target for further investigation and exploration. Possible geological and geomorphological indicators of magma–water

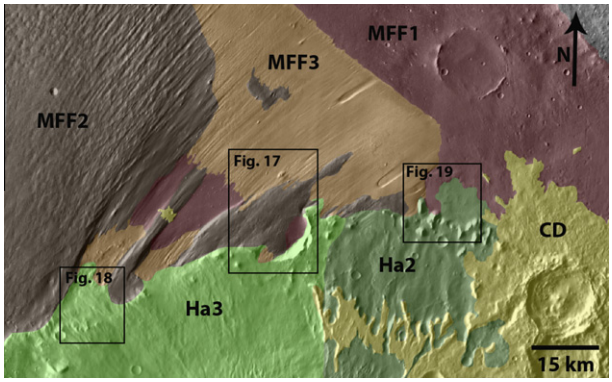

Fig. 16. Simplified colorized map showing the result of the mapping efforts carried out in this study of the various geological units comprising the northern MFF deposits and the northern flank of Apollinaris Mons overlain on a Day-time IR THEMIS mosaic. Three different MFF units can be discerned on account of differences in morphology, texture, and stratigraphy with unit MFF3 being the youngest unit and MFF1 the oldest (and acting as basement in this figure). This stratigraphical relation is also evident through elevation data with MFF3 unit being the highest topographically. The transitions from one unit to another are usually gradational although some locations display sharp transitions. The chronological relation between the MMF deposits and the flank material (Ha2 and Ha3) is complex while the crater deposits (CD) vary in age depending on the particular impact event creating the deposits.

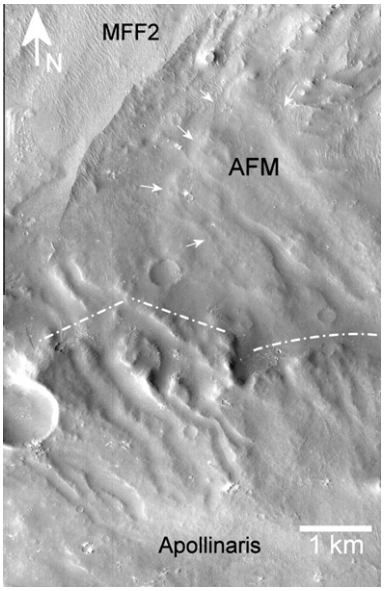

Fig. 18. CTX image of another contact between MMF and the main edifice. Young Apollinaris flow materials (AFMs) appear to have draped and extended beyond the edifice's scarp and are now overlying the MFF deposits interpreted in this study as MFF2 unit. Image ID: B12_014132_1721.

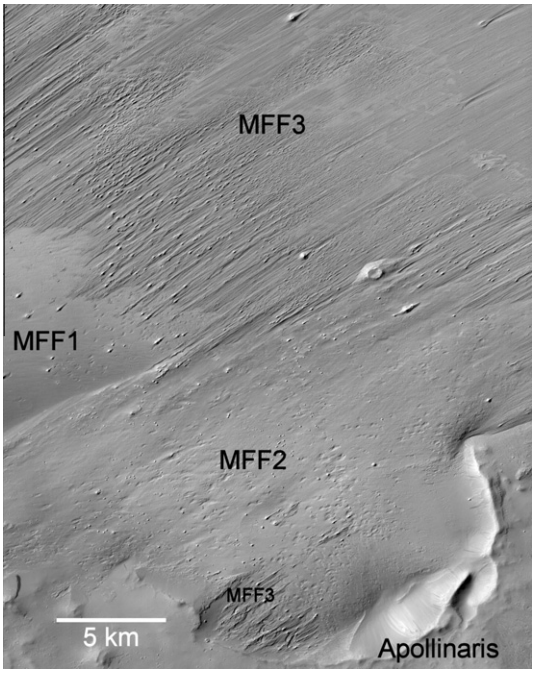

Fig. 17. CTX image of one of the contacts between Apollinaris and the MFF deposits. The three units can be seen along with their stratigraphical relations. MFF3 unit shows features interpreted as yardangs as is common for MFF. Mounds appear scattered throughout all the units. Image ID: P16_007236_1754.

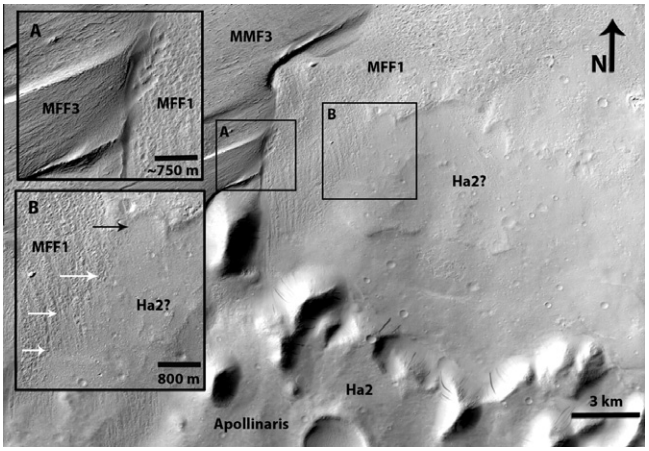

Fig. 19. CTX image of the Ha2 unit's contact with the MFF deposits. Important features to note are the sharp unconformity between MFF3 and MFF1 units (inbox A), and the extent of the Ha2 Unit at the base of volcano to the north where it overlies the MFF1 unit (inbox B, white arrows) and appears to have embayed a small 700 m-impact crater on the MFF1 unit (inbox B, black arrow). Finally, note the presence of various slope streaks on various slopes at the bottom of the image. On the basis of these relations we interpret that differential erosion has removed an old deposit (possibly MFF2) overlying the MFF1 creating the unconformity with the MFF3 unit. This was followed by the deposition of the reworked or slumped Ha2 material (possibly through mass-wasting processes). Image ID: B17_016255_1733.

interaction include the presence of mounds, possible lahar events, ubiquitous presence of impact craters with fluidized ejecta, and aqueous indicators at the caldera complex that include large rampart craters, dark streak slopes (if liquid water is involved in their formation), and possible density currents. In the following sections, the presented data is discussed with regards to alternative hypotheses and the general implications for the results presented in this work.

7.1. Formation mechanism(s) of the mounds: competing hypotheses

The geomorphological principle of equifinality makes it very difficult to distinguish between various processes to explain the formation mechanism of the mounds discussed in Section 3.2. The additional data from thermal inertia may lead to constraining the possible processes; these values, while being generally low and contra-indicative of fresh rocks, cannot rule out a volcanic (cinder cones or cryptodomes) or hydro/glacio-volcanic (e.g., rootless cones, tuff cones, maars, tuyas) origin for the mounds because relatively fresh solidified lava flow and pyroclastic (e.g., bombs)

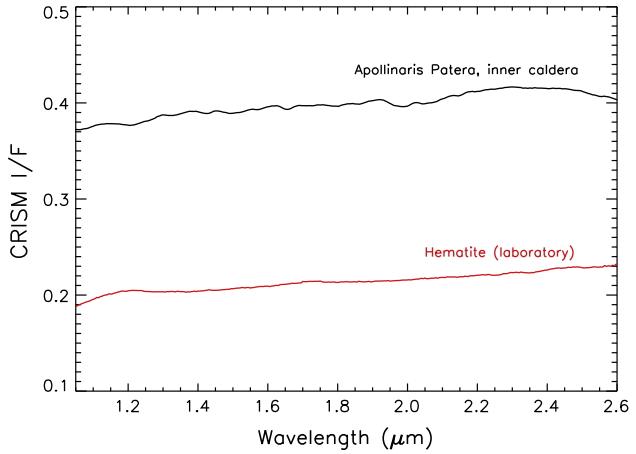

Fig. 20. A CRISM spectra from Apollinaris inner caldera (black). As discussed in the text, the spectra are fairly featureless with a slight positive slope that could be indicative of iron oxides. As a comparison, a lab spectrum of hematite at the same spectral range (red) is shown. CRISM image ID: HRL0000C68B, Hematite lab spectrum: CRISM spectral library, Sample ID: CAGR04. (For interpretation of the references to color in this figure legend, the reader is referred to the web version of this article.)

materials are expected to yield relatively higher thermal inertia values when compared to surrounding materials which is indeed observed irrespective of the absolute low values that can be due to the presence of a dust cover. However, tuff cones and maars are usually characterized by large vent to base diameter ratios (~0.5, see Farrand et al., 2005) as a result of their explosive formation. Similar to their possible terrestrial counterparts, large vent structures which occur in the northern MFF deposits (Fig. 8g) have vent to base diameter ratios of ~0.7. The rest of the mounds in the Apollinaris Mons region, however, exhibit an order of magnitude smaller ratio (0.09 on average).

Non-volcanic candidates are also possible such as mud volcanoes, pingos, and piping structures formed from the migration of fluids such as springs. Mud volcanoes are the result of gas discharge which is usually accompanied with non-explosive effusion of soft and wet sediments. Some mud volcanoes on Earth are known to reach diameters of 4 km and heights of ~500 m such as the ones in northern Irian Java, New Guinea (Williams et al., 1984), and the submarine Gelendzhik mud plateau in the crest of the Mediterranean Ridge (Limonov et al., 1996) in addition to exhibiting small pits or vents. As such, a mud volcano origin for the Apollinaris Mons mounds is a strong possibility. Mud volcanoes, for example, should exhibit low thermal inertia, similar to the Apollinaris Mons mounds as noted above. Indeed, our thermal inertia values correlate well with previous estimates of putative mud volcanoes in Acidalia Planitia and Cydonia Mensae (Farrand et al., 2005). Additionally, some mounds exhibit flow features similar to those associated with mud volcanoes on Earth and possible mud volcanoes on Mars (Fig. 8d and e) (Oehler and Allen, 2010; Komatsu et al., 2011), however, the mounds do not appear to be associated with sedimentary basins.

Pingos are small hills with cores of ice in periglacial environments, formed by the injection and freezing of pressurized water (Dundas and McKewen, 2010). Though they have similar dimensions to the ones in the Apollinaris Mons region, there are several reasons why a pingo origin is unlikely. For example, whereas pingos usually often exhibit radial fractures due to its growth, such features have not been observed in the Apollinaris mounds. In addition, the surfaces of terrestrial pingos are composed of the same materials as their surroundings, therefore exhibiting uniform albedo and thermal properties, which is not the case for the Apollinaris Mons mounds. Finally, other periglacial features associated with Apollinaris have yet to be identified using existing data, though the terraces and slide materials along the margins of the mesas of the chaotic terrain and channel system located to the south–southwest of the prominent volcano may hint at periglacial-related processes. A pingo origin cannot be entirely ruled out, especially since Apollinaris Mons and its surroundings record a geologic record that points to long-term water enrichment as shown here and noted by Scott et al. (1993).

Finally, both hot and cold springs can form extensive evaporite deposits around their sources. Hot springs can also erupt water in the form of geysers. As described and interpreted in Vernal crater of the Arabia Terra region (Allen and Oehler, 2008), geysers and springs can have various shapes and sizes similar to the ones in Apollinaris Mons region. On Earth, they can display pits at their summits, and they usually have high albedos on account of their mineralogy with respect to the hot ejected materials. As a result, springs and geysers may be good candidates for the smaller mounds.

In conclusion, the distribution and variable morphologies of mounds in the Apollinaris Mons region suggests multiple formation mechanisms, with most of them pointing to hydrothermal, phreatic, or glacio-volcanic activity. The spatial association among other features such as faults and fractures and materials such as those that compose the construct and the chaotic terrain and MFF suggests that there is likely more than one progenitor with many candidate mechanisms indicating volatile enrichment at some time in the past as well as a complex geological history.

7.2. Fan deposits and Ha2 flank material as possible lahars

Volcanic mudflows (lahars) have been documented on Earth where eruptions have occurred in water/ice-rich zones, some with catastrophic results. Lahars can be produced through five mechanisms (Major and Newhall, 1989; Lecointre et al., 2004): (1) scouring and melting by flowing pyroclastic material, (2) surficial melting by lava flows, (3) basal melting of glaciers and snow packs through subglacial eruptions or geothermal activity, (4) ejection of water by eruption through a crater lake, and (5) deposition of tephra deposits on ice packs thereby decreasing their albedo and enhancing melting, which can later be remobilized by rainfall. On Mars, records of significant water enrichment and magmatism are often interrelated (Dohm et al., 1998, 2009a,b), and the formation of lahars associated with the growth of volcanoes such as Apollinaris Mons are envisaged. Indeed, the Elysium region northwest of Apollinaris contains similar features that have been identified as lahars (Christiansen, 1989; Russell and Head, 2003). While a lahar origin for the fan deposits has already been forwarded by various workers prior to this study, this work adds strength to this hypothesis while also pointing to another possible lahar event affecting the Ha2 unit.

In the case of the fan deposits, the newly presented MOLA estimates of the bulk thickness of the deposits coupled with the presence of km-sized impact craters with fluidized ejecta argue for a non-volcanic origin. In particular, a 5-km impact crater with fluidized ejecta has most likely excavated material solely from within the fan deposits (M4 profile in Fig. 3) implying a fluid-rich composition. It is possible that further analysis of radar measurements on the fan deposits (El Maarry et al., 2011) will yield a more accurate interpretation of the composition of this geological unit as well as its extent.

On the other hand, the distinctive unit on the NE flank (Ha2) has been previously mapped and described as a volcanic unit of Apollinaris Mons that underlies more extensive flank-forming materials, also described as a volcanic unit (unit Ha3). The Ha2 unit contains a 5-km-sized impact crater with highly deformed

fluidized ejecta material. In addition, the unit appears smoother than the adjacent (stratigraphically younger) volcanic materials, comprising mostly subdued impact craters. At the bottom of the flank, many km-sized blocks appear to have slumped from the flank-forming materials (Fig. 5). Narrow valleys are evident (though at times subdued) in many locations resembling seepage channels with no clear tributaries or distributaries. Based on high-resolution images, the Ha2 deposits appear to overly what are interpreted to be MFF deposits (Fig. 15), a stratigraphic relation which has already been reported with the Ha2 deposits, referred to as simply "Apollinaris materials" by Kerber and Head (2010), forming distinctive elevated margins markedly on the western side of the deposits (Fig. 15). This stratigraphic relation indicates that there was time separation between the emplacement of the older, flank-forming materials and the event which resulted in the distinctive materials, unit Ha2. Mass movement such as a lahar and associated morphologic expression could have been initiated through a number of processes such as the interaction of snow/liquid water and volcanism or impact-generated tectonic instability and related geothermal activity associated with the formation of two relatively large craters (18 and 20 km in diameter) located 30 km to the east of the unit.

In conclusion, numerous indicators in support of the lahar hypothesis include (1) evidence for water activity through seepage channels, (2) evidence for mass-wasting through the degradation of the rampart ejecta of nearby impact craters and presence of slumped material, (3) presence of distinctly elevated margins and (4) the apparent smoothness of the deposits (Siebert, 1984; Christiansen, 1989). However, the lack of other indicators such as multiple overlapping lobes, clear lateral deposits, and flow fronts make lahar interpretation for these deposits speculative. Finally, while the young ages given by crater counts of this study corroborates the hypothesis that the lahar flow has covered the older unit at a later stage masking a significant number of the older impact craters, alternatively, the unit's deviation in crater statistics could indicate that the deposits are more friable than the neighboring volcanic units and thus readily degraded by processes such as wind or hydrologic erosion.

7.3. A possible caldera paleolake?

There are multiple indicators that hint at the past existence of a volcanic lake at the summit of Apollinaris Mons, including: (1) the evidence of near surface enrichment in volatiles as indicated by the impact craters with fluidized ejecta inside the inner caldera complex, (2) the presence of putative major lahar events that appear to initiate from the summit, and (3) similarity to hydrothermal/magmatic systems on Earth with an associated volcanic lake.

Volcanic lakes are a common feature in many hydrothermal/magmatic systems on Earth ranging in composition from very dilute meteoric waters to highly acidic (<0.5 pH) brines. They can either have a purely meteoric origin or a hydrothermal/magmatic one, but mostly, they are a combination of both, forming through interaction of magmatic fluids with ground water (Varekamp et al., 2000). There are numerous examples for hydrothermal/magmatic-induced lakes such as the ones at Mt. Ruapehu, New Zealand (Christenson, 2000), Kawah Ijen, Indonesia (Delmelle et al., 2000), Poás volcano, Costa Rica (Rowe et al., 1992), Copahue volcano, Argentina (Varekamp et al., 2004), and the Waimangu system, New Zealand (Scott, 1995) with Mt. Ruapehu being an interesting example where its caldera lake is reported to have created multiple lahar events through breaching of the caldera with devastating consequences during the past 2000 years (Lecointre et al., 2004; Kilgour et al., 2010).

Another notable example is the Copahue volcano which has been cited as a possible modern terrestrial analog for the MER Opportunity landing site (Varekamp, 2004) since the region contains an acid lake and hot springs that deposit jarosite, gypsum, and hematite; a suite of minerals detected by Opportunity at Terra Merdiani (Christensen et al., 2001; Hynek et al., 2002; Klingelhöfer et al., 2004). In addition, the Copahue environment can exist without a meteoric water cycle, since the hot spring fluids are 50–70% magmatic waters that are quenched by meltwater supplied from the summit glacier of Copahue (Varekamp, 2004). Such an environment is highly plausible for Apollinaris Mons in presumed periods of activity while a similar geologic history to Mt. Ruapehu may aptly explain many features associated with Apollinaris Mons.

The suite of findings discussed in the previous sections points to a possible period of magma/water interaction making it likely that such a lake would have formed at the summit of Apollinaris Mons. An Apollinaris lake would have persisted for a significant amount of time even under conditions similar to Mars today. The same arguments that have been put forward to show the longevity of impact-driven hydrothermal lakes (Newsom et al., 1996; Abramov and Kring, 2005) apply even more so for magmatic-driven ones which are expected to exhibit longer lifetimes.

On Earth, volcanic lakes can reach temperatures of 70–80 °C as a result of the heat influx from the magmatic parent body, fluid circulation, and fumarolic activity. On Mars, ambient temperatures are generally lower than Earth. Nevertheless, it is expected that magmatic activity would be capable of keeping the lake temperature above the freezing point for most of its activity. Any extensive magmatic episodes occurring in the vicinity of the lake would have breached the caldera rim triggering an overflow and possibly a lahar event similar to what was witnessed at Mt. Ruapehu in 2007 (Kilgour et al., 2010).

Finally, it should be noted that Ghail and Hutchison (2003) were the first to suggest the past existence of a volcanic lake at the summit of Apollinaris Mons based on their interpretation of the fan deposits covering its southern flank as alluvial in origin. Their interpretation was based on existing high-resolution data that did not reveal features usually associated with volcanic flows as was originally predicted by Robinson et al. (1993) and Scott et al. (1993). Though differentiating among the proposed explanations for the fan deposits (i.e., volcanic flow, alluvial fan, or ignimbrites) is tenuous using geomorphology alone, radar data may help constrain these possibilities. Preliminary analysis of Shallow Radar (SHARAD; Seu et al., 2007) data indicates that the fan deposits are layered, which suggests long-term periodical activity (El Maarry et al., 2011).

7.4. Implication for exobiology

The diverse evidence of past and present-day water/ice at the martian surface, coupled with the dynamic geologic history as noted above, indicates that hydrothermal environments existed in the past and some may still be active today (Dohm et al., 1998, 2008; Mustard et al., 2006; Schulze-Makuch et al., 2007). These environments are considered prime targets for testing the hypothesis of whether life existed (or still exists) on Mars (Dohm et al., 2004). Assessing the past existence of hydrothermal systems on Mars has important astrobiological implications because hydrothermal systems may have provided habitats for the origin and evolution of early life (Shock, 1996; Farmer, 2000; Schrenk et al., 2010). On Earth, life strives in hydrothermal environments with low pH and temperatures close to the boiling point of water. Prokaryotes, which have dominated life on Earth for most of Earth's history, have adapted to environmental extremes of temperature, pH, pressure, salinity, and anoxic conditions (e.g., Nealson, 1999; Schulze-Makuch and Irwin, 2004).

It is possible that hydrothermal environments on Mars may also record biologic activity assuming that life began there. On Mars,

such environments (Dohm et al., 2008) may have been extremely long-lived as in the case of Apollinaris Mons, for example, which was potentially active from the Late Noachian Epoch through the Late Hesperian Epoch. As a result, we propose that the mound structures around Apollinaris should be prime targets for future landed missions to search for exobiological signatures in the area since they meet the scientific requirements of being strong candidates for evidence of magma/water interaction.

8. Conclusion

Our investigation using recently acquired remote sensing data supports the Viking-era geologic investigations which pointed to Apollinaris Mons (formerly Apollinaris Patera) as a site of extensive volcanic and hydrologic activity with possibly a period of magma–water interaction. The main findings include:

(1) Evidence from laser altimetry indicating the large thickness (1.5–2 km at some locations) of the fan deposits coupled with possible layering which point to a significant emplacement phase of Apollinaris Mons, a marker for a far-reaching history associated with the development of the prominent and seemingly isolated volcano, including long-term magmatic activity, and possibly, magma–water interaction.
(2) Corroboration of Robinson et al. (1993) hypothesis regarding the formation of incised valleys on the western flanks by density current erosion which would indicate magma–water interaction or, alternatively, volatile-rich magmas early in the volcano's history.
(3) Numerous faults, fractures, and scarps possibly related to magmatic-driven tectonism, which were not observed during Viking-era geologic mapping investigations.
(4) Mounds of diverse geometric shapes, many of which display summit depressions and occur among faults and fractures, possibly marking venting.
(5) A valley system, which dissects Medusae Fossae materials to the east of the volcano, is traced more accurately corroborating the previous assumptions that the system marks geologically recent liquid water activity on the martian surface.
(6) Ubiquitous presence of impact craters in both shield-forming (flank and caldera) materials and materials that surround the volcano that are indicative of water-rich target materials at the time of impact such as impact layered ejecta deposits.
(7) Long-term association in time among shield-forming materials and Medusae Fossae Formation.
(8) Strong indicators on the flanks of the volcano for lahar events, and possibly, a caldera paleolake.

These results also point to Apollinaris Mons being a site of exobiological significance, which includes the mound-like features as prime candidate targets to test whether life existed on Mars.

Acknowledgments

M.R. El Maarry was supported by an MPG-IMPRS Grant. James M. Dohm was funded through NASA's Mars Data Analysis Program. The first author would like to thank Johan Verkamp for his clarifications on the nature and evolution of volcanic lakes on Earth, and Roberto Bugiolacchi for his valuable comments. We would also like to thank two anonymous reviewers for their critical comments and suggestions that greatly improved this paper.

Appendix A. Supplementary material

Supplementary data associated with this article can be found, in the online version, at doi:10.1016/j.icarus.2011.10.022.

References

Abramov, O., Kring, D.A., 2005. Impact-induced hydrothermal activity on early Mars. J. Geophys. Res. 110, E12S09. doi:10.1029/2005JE002453.
Allen, C.C., 1979. Areal distribution of martian rampart craters. Icarus 39, 111–123.
Allen, C.C., Oehler, D.Z., 2008. A case for ancient springs in Arabia Terra, Mars. Astrobiology 8, 1093–1112.
Anderson, R.C. et al., 2001. Significant centers of tectonic activity through time for the western hemisphere of Mars. J. Geophys. Res. 106, 20563–20585.
Anderson, R.C. et al., 2008. Centers of tectonic activity in the eastern hemisphere of Mars. Icarus. doi:10.1016/j.icarus.2007.12.027.
Arvidson, R.E. et al., 1976. Latitudinal variation of wind erosion of crater ejecta deposits on Mars. Icarus 27, 503–516. doi:10.1016/0019-1035(76)90166-4.
Arvidson, R.E. et al., 2006. Overview of the Spirit Mars Exploration Rover Mission to Gusev Crater: Landing site to Backstay Rock in the Columbia Hills. J. Geophys. Res. 111, E02S01. doi:10.1029/2005JE002499.
Arvidson, R.E. et al., 2008. Spirit Mars Rover Mission to the Columbia Hills, Gusev Crater: Mission overview and selected results from the Cumberland Ridge to Home Plate. J. Geophys. Res. 113, E12S33. doi:10.1029/2008JE003183.
Arvidson, R.E. et al., 2010. Spirit Mars Rover Mission: Overview and selected results from the northern Home Plate Winter Haven to the side of Scamander crater. J. Geophys. Res. 115, E00F03. doi:10.1029/2010JE003633.
Baker, V.R., Milton, D.J., 1974. Erosion by catastrophic floods on Mars and Earth. Icarus 23, 27–41.
Baker, V.R., Strom, R.G., Gulick, V.C., Kargel, J.S., Komatsu, G., Kale, V.S., 1991. Ancient oceans, ice sheets, and the hydrological cycle on Mars. Nature 352, 589–594.
Barlow, N.G., 2004. Martian subsurface volatile concentrations as a function of time: Clues from layered ejecta craters. Geophys. Res. Lett. 31, L05703. doi:10.1029/2003GL019075.
Barlow, N.G., Bradley, T.L., 1990. Martian impact craters: Correlations of ejecta and interior morphologies with diameter, latitude, and terrain. Icarus 87, 156–179.
Barlow, N.G. et al., 2000. Standardizing the nomenclature of martian impact crater ejecta morphologies. J. Geophys. Res. 105 (E11), 26733–26738.
Barlow, N.G., Koroshetz, J., Dohm, J.M., 2001. Variations in the onset diameter for martian layered ejecta morphologies and their implications for subsurface volatile reservoirs. Geophys. Res. Lett. 28 (16), 3095–3098. doi:10.1029/2000GL012804.
Bleacher, J.E., Wet, A.P., Garry, W.B., Zimbelman, J.R., Trumble, M.E., 2010. Volcanic or fluvial: Comparison of an Ascraeus Mons, Mars, braided and sinuous channel with features of the 1859 Mauna Loa flow and Mare Imbrium flows. Lunar Planet. Sci. 41. Abstract #1612.
Boynton, W.V. et al., 2004. The Mars Odyssey Gamma-Ray Spectrometer instrument suite. Space Sci. Rev. 110, 37–83.
Carr, M., 1979. Formation of martian flood features by release of water from confined aquifers. J. Geophys. Res. 84 (B6), 2995–3007. doi:10.1029/JB084iB06p02995.
Carr, M.H., 1986. Mars: A water rich planet? Icarus 68, 187–216.
Carr, M.H., Crumpler, L.S., Cutts, J.A., Greeley, R., Guest, J.E., Masursky, H., 1977. Martian impact craters and emplacement of ejecta by surface flow. J. Geophys. Res. 82, 4055–4065.
Chioni, R., Corazza, E., Marini, L., 1984. The gas/steam ratio as indicator of heat transfer at the Solfatara Fumarole, Phlegrean Fields (Italy). Bull. Volcanol. 47, 295–302.
Christensen, P.R. et al., 2001. Mars Global Surveyor thermal emission spectrometer experiment: Investigation description and surface science results. J. Geophys. Res. 111, 23823–23872.
Christensen, P.R. et al., 2004. The Thermal Emission Imaging System (THEMIS) for the Mars 2001 Odyssey mission. Space Sci. Rev. 101, 85–130.
Christenson, B.W., 2000. Geochemistry of fluids associated with the 1995/96 eruption of Mt. Ruapehu, New Zealand: Signatures and processes in the magmatic–hydrothermal system. J. Volcanol. Geotherm. Res. 97, 1–30.
Christiansen, E.H., 1989. Lahars in the Elysium region of Mars. Geology 17, 203–206.
Chuang, F.C., Beyer, R.A., McEwen, A.S., Thomson, B.J., 2007. HiRISE observations of slope streaks on Mars. Geophys. Res. Lett. 34, L20204. doi:10.1029/2007GL031111.
Clifford, S.M., Parker, T.J., 2001. The evolution of the martian hydrosphere: Implications for the fate of a primordial ocean and the current state of the northern plains. Icarus 154, 40–79.
Crown, D.A., Greeley, R., 1993. Volcanic geology of Hadriaca Patera and the eastern Hellas region of Mars. J. Geophys. Res. 98 (E2), 3431–3451. doi:10.1029/92JE02804.
Crown, D.A., Bleamaster III, L.F., Mest, S.C., 2005. Styles and timing of volatile-driven activity in the eastern Hellas region of Mars. J. Geophys. Res. 110, E12S22. doi:10.1029/2005JE002496.
Crumpler, L.S., Head, J.W., Aubele, J.C., 1996. Calderas on Mars: Characteristics, structure and associated flank deformation. In: McGuire, W.J., Jones, A.P.,

Neuberg, J. (Eds.), Volcano Instability on the Earth and Other Planets, vol. 110. Geol. Soc. Spec. Publ., pp. 307–348.
Delmelle, P., Bernard, A., Kusakabe, M., Fischer, T., Takano, B., 2000. Geochemistry of the magmatic-hydrothermal system of Kawah Ijen volcano, East Java, Indonesia. J. Volcanol. Geotherm. Res. 97, 31–53.
Di Achille, G., Hynek, B.M., 2010. Ancient ocean on Mars supported by global distribution of deltas and valleys. Nat. Geosci. 3, 459–463.
Di Achille, G. et al., 2006. Geological evolution of the Tyras Vallis paleolacustrine system, Mars. J. Geophys. Res. 111, E04003. doi:10.1029/2005JE002561.
Dohm, J.M., 1995. Origin of Stoneman Lake, and volcano-Tectonic Relations of Mormon and San Francisco Volcanic Fields, Arizona. Thesis, Northern Arizona University, Flagstaff, Arizona.
Dohm, J.M., Anderson, R.C., Tanaka, K.L., 1998. Digital structural mapping of Mars. Astron. Geophys. 39, 3.20–3.22.
Dohm, J.M., Tanaka, K.L., Hare, T.M., 2001a. Geologic Map of the Thaumasia Region of Mars. US Geol. Survey Map I-2650.
Dohm, J.M. et al., 2001b. Ancient drainage basin of the Tharsis region, Mars: Potential source for outflow channel systems and putative oceans or paleolakes. J. Geophys. Res. 106, 32942–32958.
Dohm, J.M. et al., 2004. The Northwestern Slope Valleys (NSVs) region, Mars: A prime candidate site for the future exploration of Mars. Planet. Space Sci. 52, 189–198.
Dohm, J.M. et al., 2007. Possible ancient giant basin and related water enrichment in the Arabia Terra province, Mars. Icarus 190, 74–92. doi:10.1016/j.icarus.2007.03.006.
Dohm, J.M. et al., 2008. Recent geological and hydrological activity on Mars: The Tharsis/Elysium Corridor. Planet. Space Sci. 56, 985–1013.
Dohm, J.M. et al., 2009a. GRS evidence and the possibility of ancient oceans on Mars. Planet. Space Sci. 57, 664–684.
Dohm, J.M. et al., 2009b. New evidence for a magmatic influence on the origin of Valles Marineris, Mars. J. Volcanol. Geotherm. Res. 185, 12–27.
Dundas, C.M., McKewen, A.S., 2010. An assessment of evidence for pingos on Mars using HiRISE. Icarus 205, 244–258.
El Maarry, M.R., Markiewicz, W.J., Mellon, M.T., Goetz, W., Dohm, J.M., Pack, A., 2010. Crater floor polygons: Desiccation patterns of ancient lakes on Mars? J. Geophys. Res. 115, E10006. doi:10.1029/2010JE003609.
El Maarry, M.R., Heggy, E., Dohm, J.M., 2011. Assessment of a possible volcanic Paleolake at Apollinaris Patera, Mars: Constraints on the Composition of the inner caldera and fan deposits using the shallow sounding radar (SHARAD). Lunar Planet. Sci. 42. Abstract #2027.
Fairén, A.G. et al., 2003. Episodic flood inundations of the northern plains of Mars. Icarus 165, 53–67.
Fairén, A.G. et al., 2010. Noachian and more recent phyllosilicates in impact craters on Mars. Proc. Natl. Acad. Sci. 107, 12095–12100.
Farmer, J.D., 1996. Hydrothermal processes on Mars: An assessment of present evidence. In: Gregory, Bock, Jamie, Goode (Eds.), Evolution of Hydrothermal Ecosystems on Earth (and Mars?). John Wiley and Sons, pp. 273–299.
Farmer, J.D., 2000. Hydrothermal systems: Doorways to early biosphere evolution. Geol. Soc. Am. Today 10, 1–9.
Farrand, W.H., Gaddis, L.R., Keszthelyi, L., 2005. Pitted cones and domes on Mars: Observations in Acidalia Planitia and Cydonia Mensae using MOC, THEMIS, and TES data. J. Geophys. Res. 110, E05005. doi:10.1029/2004JE002297.
Farrand, W.H., Lane, M.D., Edwards, B.R., Yingst, R.A., 2010. Spectral evidence of volcanic cryptodomes on the northern plains of Mars. Icarus 221, 139–156.
Farrell, A.K., Lang, N.P., 2011. Distribution of explosive and effusive volcanic deposits at Apollinaris Patera, Mars. Lunar Planet. Sci. 41. Abstract #2072.
Fergason, R.L., Christensen, P.R., Kieffer, H.H., 2006. High-resolution thermal inertia derived from the Thermal Emission Imaging System (THEMIS): Thermal model and applications. J. Geophys. Res. 111, E12004. doi:10.1029/2006JE002735.
Ferguson, H.M., Lucchitta, B.K., 1983. Dark streaks on talus slopes, Mars. NASA Tech. Memo. 86246, 188–190.
Ferris, J.C., Dohm, J.M., Baker, V., Maddock, T., 2002. Dark slope streaks on Mars: Are aqueous processes involved? Geophys. Res. Lett. 29 (10). doi:10.1029/2002GL014936.
Fulton, R.J., 1989. Quaternary Geology of Canada and Greenland. Geological Survey of Canada, 1–11 and 99.
Gellert, R. et al., 2004. Chemistry of rocks and soils in Gusev Crater from the Alpha Particle X-ray Spectrometer. Science 305, 829–832.
Ghail, R.C., Hutchison, J.E., 2003. An alluvial fan at Apollinaris, Mars. Lunar Planet. Sci. 34. Abstract #1775.
Glamoclija, M., Garrel, L., Berthon, J., López-García, P., 2004. Biosignatures and bacterial diversity in hydrothermal deposits of Solfatara Crater, Italy. Geomicrobiol. J. 21, 529–541.
Greeley, R. et al., 2005. Fluid lava flows in Gusev Crater, Mars. J. Geophys. Res. 110, E05008. doi:10.1029/2005JE002401.
Greg, T.K.P., Crown, D.A., Sakimoto, S.E.H., 2002. Volcanic Evolution and Erosion at Tyrrhena and Hadriaca Paterae, Mars. Lunar Planet Sci. XXXIII. Abstract #1560.
Gregg, T.K.P., Krysak, D.J., 2011. Apollinaris Mons, Mars: A new name and a new past. Lunar Planet. Sci. Abstract #1922.
Grizzaffi, Patricia, Schultz, P.H., 1989. Isidis basin: Site of ancient volatile-rich debris layer. Icarus 77, 358–381.
Gulick, V.C., 1998. Magmatic intrusions and a hydrothermal origin for fluvial valleys on Mars. J. Geophys. Res. 103 (E8), 19365–19387.
Gulick, V.C., 2001. Origin of the valley networks on Mars: A hydrological perspective. Geomorphology 37, 241–268.
Gulick, V., Baker, V., 1989. Fluvial valleys and martian paleoclimates. Nature 341, 514–516.
Gulick, V., Baker, V., 1990. Origin and evolution of valleys on martian volcanoes. J. Geophys. Res. 95 (B9), 14325–14344.
Hapke, B., 1981. Bidirectional reflectance spectroscopy. 1. Theory. J. Geophys. Res. 86, 4571–4586.
Hartmann, W.K., Neukum, G., 2001. Cratering chronology and the evolution of Mars. Space Sci. Rev. 96, 165–194.
Hock, A.N. et al., 2007. Scoring system for habitability and the robotic exploration for life. J. Geophys. Res. 112, G04S08. doi:10.1029/2006JG000321.
Hodges, C.A., Moore, H.J., 1994. Atlas of Volcanic Landforms on Mars: US Geol. Surv. Prof. Pap. 1534.
Holm, R.F., 2001. Cenozoic paleogeography of the central Mogollon Rim–southern Colorado Plateau region, Arizona, revealed by Tertiary gravel deposits, Oligocene to Pleistocene lava flows, and incised streams. Geol. Soc. Am. Bull. 113, 1467–1485.
Hood, L.L. et al., 2010. Magnetic anomalies near Apollinaris Patera and the Medusae Fossae Formation in Lucus Planum, Mars. Icarus 208, 118–131.
Hynek, B.M., Arvidson, R.E., Phillips, R.G., 2002. Geologic setting and origin of Terra Meridiani hematite deposit on Mars. J. Geophys. Res. 107. doi:10.1029/2002JE001891.
Ivanov, B.A., 2001. Mars/Moon cratering rate ratio estimates. Space Sci. Rev. 96, 87–104. doi:10.1023/A:1011941121102.
Kargel, J.S., 2004. Mars: A Warmer Wetter Planet. Praxis-Springer.
Kargel, J.S., Strom, R.G., 1992. Ancient glaciation on Mars. Geology 20, 3–7.
Keller, J.M. et al., 2006. Equatorial and midlatitude distribution of chlorine measured by Mars Odyssey GRS. J. Geophys. Res. 111, E03S08. doi:10.1029/2006JE002679.
Kerber, L., Head, J.W., 2010. The age of the Medusae Fossae Formation: Evidence of Hesperian emplacement from crater morphology, stratigraphy, and ancient lava contacts. Icarus 206, 669–684.
Kieffer, S.W., Simonds, C.H., 1980. The role of volatiles and lithology in the impact cratering process. Rev. Geophys. 18, 143–181.
Kilgour, G., Manville, V., Della Pasqua, F., Graettinger, A., Hodgson, K.A., Jolly, G.E., 2010. The 25 September 2007 eruption of Mount Ruapehu, New Zealand: Directed ballistics, surtseyan jets, and ice-slurry lahars. J. Volcanol. Geotherm. Res. 191, 1–14.
Klingelhöfer, G. et al., 2004. Jarosite and hematite at Meridiani Planum from Opportunity's Mössbauer Spectrometer. Science 306, 1740–1745.
Komatsu, G. et al., 2011. Roles of methane and carbon dioxide in geological processes on Mars. Planet. Space Sci. 59, 169–181.
Lang, N.P., McSween, H.Y., Tornabene, L.L., Hardgrove, C.J., Christensen, P.R., 2010. Reexamining the relationship between Apollinaris Patera and the basalts of the Gusev Crater plains, Mars. J. Geophys. Res. 115, E04006. doi:10.1029/2009JE003397.
Lang, N.P., Kelley, R., Farrel, A.K., 2011. An examination of the contact between Apollinaris Patera and the Medusae Fossae Formation, Mars: Implications for Apollinaris' volcanic evolution. Lunar Planet. Sci. 42. Abstract # 1329.
Langlais, B., Purucker, M., 2007. A polar magnetic paleopole associated with Apollinaris Patera, Mars. Planet. Space Sci. 55, 270–279.
Lecointre, J., Hodgson, K., Neall, V., Cornin, S., 2004. Lahar-triggering mechanisms and hazard at Ruapehu volcano, New Zealand. Nat. Hazards 31, 85–109.
Leverington, D.W., 2004. Volcanic rilles, streamlined islands, and the origin of outflow channels on Mars. J. Geophys. Res. 109, E10011. doi:10.1029/2004JE002311.
Levy, J., Head, J., Marchant, D., 2009. Thermal contraction crack polygons on Mars: Classification, distribution, and climate implications from HiRISE observations. J. Geophys. Res. 114, E01007. doi:10.1029/2008JE003273.
Limonov, A.F., Woodside, J., Cita, M., Ivanov, M., 1996. The Mediterranean Ridge and related mud diapirism: A background. Mar. Geol. 132, 7–19.
Lucchitta, B.K., 1981. Mars and Earth: Comparison of cold-climate features. Icarus 45, 264–303.
Mahaney, W.C. et al., 2004. Ancient wet Aeolian environments on Earth: Clues to presence of fossil/live microorganisms on Mars. Icarus 171, 39–53.
Mahaney, W.C. et al., 2007. Rock glaciers on Mars: Earth-based clues to Mars' recent paleoclimatic history. Planet. Space Sci. 55, 181–192.
Major, J.J., Newhall, C.G., 1989. Snow and ice perturbation during historical volcanic eruptions and the formation of lahars and floods. Bull. Volc. 52, 1–27.
Malin, M.C., Edgett, K.S., 2001. Mars Global Surveyor Mars Orbiter Camera: Interplanetary cruise through primary mission. J. Geophys. Res. 106, 23429–23570.
Malin, M.C., Edgett, K.S., 2003. Evidence for persistent flow and aqueous sedimentation on Mars. Science 302, 1931–1934. doi:10.1126/science.1090544.
Malin, M.C. et al., 1992. Mars Observer Camera. J. Geophys. Res. 97 (E5), 7699–7718.
Malin, M.C. et al., 2007. Context Camera investigation on board the Mars Reconnaissance Orbiter. J. Geophys. Res. 112, E05S04.
Marzo, G.A. et al., 2010. Evidence for Hesperian impact-induced hydrothermalism on Mars. Icarus 208, 667–683.
Mathews, J.V., 1990. Approaching today. In: Mungall, C., McLaren, D. (Eds.), Planet under Stress: The Challenge of a Global Change. Oxford University Press and the Royal Society of Canada, Toronto, pp. 96–109.
McCauley, J., 1973. Mariner 9 evidence for wind erosion in the equatorial and mid-latitude regions of Mars. J. Geophys. Res. 78 (20), 4123–4137.
McEwen, A.S. et al., 2007. Mars Reconnaissance Orbiter's High Resolution Imaging Science Experiment (HiRISE). J. Geophys. Res. 112, E05S02. doi:10.1029/2005JE002605.

McGuire, P.C. et al., 2009. An improvement to the volcano-scan algorithm for atmospheric correction of CRISM and OMEGA spectral data. Planet. Space Sci. 57, 809–815.
Michael, G.G., Neukum, G., 2010. Planetary surface dating from crater size–frequency distribution measurements: Partial resurfacing events and statistical age uncertainty. Earth Planet. Sci. Lett. doi:10.1016/j.epsl.2009.12.041.
Miyamoto, H., Dohm, J.M., Beyer, R.A., Baker, V.R., 2004. Fluid dynamical implications of anastomosing slope streaks on Mars. J. Geophys. Res. 109, E06008. doi:10.1029/2003JE002234.
Mouginis-Mark, P.J., 1979. Martian fluidized crater morphology: Variations with crater size, latitude, altitude, and target material. J. Geophys. Res. 84 (B14), 8011–8022.
Mouginis-Mark, P.J., 1987. Water or ice in the martian regolith? Clues from rampart craters seen at very high resolution. Icarus 71 (2), 268–286.
Mouginis-Mark, P.J., 1990. Recent water release in the Tharsis region of Mars. Icarus 84, 362–373.
Murchie, S. et al., 2007. Compact Reconnaissance Imaging Spectrometer for Mars (CRISM) on Mars Reconnaissance Orbiter (MRO). J. Geophys. Res. 112, E05S03. doi:10.1029/2006JE002682, 2007.
Murchie, S.M. et al., 2009. A synthesis of martian aqueous mineralogy after one Mars year of observations from the Mars Reconnaissance Orbiter. J. Geophys. Res. 114, E00D06. doi:10.1029/2009JE003342.
Mustard, J.F., Hays, J.E., 1997. Effects of Hyperfine Particles on Reflectance Spectra from 0.3 to 25 μm. Icarus 125, 145–163.
Mustard, J.F., Poulet, F., Mangold, N., Bibring, J.-P., Milliken, R.E., Pelkey, S., 2006. Aqueous alteration and evidence of habitability in Nili Fossae: Abstract. In: First Landing Site Workshop for the 2009 Mars Science Laboratory, May 31–June 2, 2006, Pasadena, CA.
Nealson, K.H., 1999. The Search for Extraterrestrial Life: Engineering & Science, vol. LXII. California Institute of Technology (pp. 31–40).
Newsom, H.E., 1980. Hydrothermal alteration of impact melt sheets with implications to Mars. Icarus 44, 207–216.
Newsom, H.E., Brittelle, G.E., Hibbitts, C.A., Crossey, L.J., Kudo, A.M., 1996. Impact crater lakes on Mars. J. Geophys. Res. 101 (E6), 14951–14955. doi:10.1029/96JE01139.
Newsom, H.E., Hagerty, J.J., Thorsos, I.E., 2001. Location and sampling of aqueous and hydrothermal deposits in martian impact craters. Astrobiology 1, 71–88.
Oberbeck, V.R., 2009. Layered ejecta craters and the early water/ice aquifer on Mars. Meteorit. Planet. Sci. 44, 43–54.
Oehler, D.Z., Allen, C.C., 2010. Evidence for pervasive mud volcanism in Acidalia Planitia, Mars. Icarus 208, 636–657.
Ori, G.G., Marinangeli, L., Baliva, A., 2000a. Terraces and Gilbert-type deltas in crater lakes in Ismenius Lacus and Memnonia (Mars). J. Geophys. Res. 105, 17629–17642.
Ori, G.G., Marinangeli, L., Komatsu, G., 2000b. Gas (methane?) – Related features on the surface of Mars and subsurface reservoirs. Lunar Planet. Sci. 31. Abstract #1550.
Parente, M., 2008. A new approach to denoising CRISM images. Lunar Planet. Sci. 39. Abstract #2528.
Parnell, J. et al., 2010. Sulfur isotope signatures for rapid colonization of an impact crater by thermophilic microbes. Geology 38, 271–274.
Pelkey, S.M. et al., 2007. CRISM multispectral summary products: Parameterizing mineral diversity on Mars from reflectance. J. Geophys. Res. 112, E08S14. doi:10.1029/2006JE002831.
Pirajno, F., 2009. Hydrothermal Processes and Mineral Systems. Springer.
Plescia, J.B., 2004. Morphometric properties of martian volcanoes. J. Geophys. Res. 109, E03003. doi:10.1029/2002JE002031.
Rampey, M.L., Milam, K.A., McSween, H.Y., Moersch, J.E., Christensen, P.R., 2007. Identity and emplacement of domical structures in the western Arcadia Planitia, Mars. J. Geophys. Res. 112, E06011.
Rathbun, J.A., Squyres, S.W., 2002. Hydrothermal systems associated with martian impact craters. Icarus 157, 362–372.
Reimers, C.E., Komar, P.D., 1979. Evidence for explosive volcanic density currents on certain martian volcanoes. Icarus 39, 88–110.
Robinson, M., Smith, M., 1995. Multi-temporal examination of the martian surface in the Apollinaris Patera region. Eos, Trans. Am. Geophys. Un. 76. Abstract #331.
Robinson, M.S., Mouginis-Mark, P.J., Zimbelman, J.R., Wu, S.S.C., Ablin, K.K., Howington-Kraus, A.E., 1993. Chronology, eruption duration, and atmospheric contribution of the martian volcano Apollinaris Patera. Icarus 104, 301–323.
Rodriguez, J.A.P. et al., 2005. Outflow channel sources, reactivation, and chaos formation, Xanthe Terra, Mars. Icarus 175, 36–57.
Rossbacher, L.A., Judson, S., 1981. Ground ice on Mars: Inventory, distribution, and resulting landforms. Icarus 45, 39–59.
Rowe, G.L., Brantley, S.L., Fernandez, M., Fernandez, J.F., Borgia, A., Barquero, J., 1992. Fluid-volcano interaction in an active stratovolcano: The volcanic lake system of Poás Volcano, Costa Rica. J. Volcanol. Geotherm. Res 49, 23–51.
Ruff, S.W. et al., 2011. Characteristics, distribution, origin, and significance of opaline silica observed by the Spirit rover in Gusev Crater, Mars. J. Geophys. Res. 116, E00F23. doi:10.1029/2010JE003767.
Russell, P.S., Head, J.W., 2003. Elysium–Utopia flows as mega-lahars: A model of dike intrusion, cryosphere cracking, and water-sediment release. J. Geophys. Res. 108 (E6), 5064. doi:10.1029/2002JE001995.
Schmidt, M.E. et al., 2008. Hydrothermal origin of halogens at Home Plate, Gusev Crater. J. Geophys. Res. 113, E06S12. doi:10.1029/2007JE003027.
Schrenk, M.O., Huber, J.A., Edwards, K.J., 2010. Microbial provinces in the subseafloor. Annu. Rev. Mar. Sci. 2, 279–304.
Schulze-Makuch, D., Irwin, L.N., 2004. Life in the Universe: Expectations and Constraints. Springer, Berlin.
Schulze-Makuch, D. et al., 2007. Exploration of hydrothermal targets on Mars. Icarus 189, 308–324.
Schwenzer, S.P., Kring, D.A., 2009. Impact-generated hydrothermal alteration on Mars: Clay minerals, oxides, zeolites, and more. Lunar Planet. Sci. 40. Abstract #1421.
Scott, B.J., 1995. Cyclic activity in the crater lakes of Waimangu hydrothermal system, New Zealand. Geothermics 23 (5/6), 555–572.
Scott, D.H., Tanaka, K.L., 1982. Ignimbrites of Amazonis Planitia region of Mars. J. Geophys. Res. 87 (B2), 1179–1190. doi:10.1029/JB087iB02p01179.
Scott, D.H., Tanaka, K.L., 1986. Geologic map of the western equatorial region of Mars. USGS Misc. Invest. Ser. Map I-1802-A.
Scott, D.H., Dohm, J., Applebee, D., 1993. Geologic map of science study area 8, Apollinaris Patera region of Mars. USGS Maps, Map I-2351.
Scott, D.H., Dohm, J.M., Rice Jr., J.W., 1995. Map of Mars showing channels and possible paleolake basins. USGS Misc. Inv. Ser. Map I-2461 (1:30,000,000).
Seu, R. et al., 2007. SHARAD sounding radar on the Mars Reconnaissance Orbiter. J. Geophys. Res. 112, E05S05. doi:10.1029/2006JE002745.
Shock, E.L., 1996. Hydrothermal systems as environments for the emergence of life. In: Evolution of Hydrothermal Ecosystems on Earth (and Mars?), Wiley, Chichester (Ciba Foundation Symposium 202), pp. 40–60.
Siebert, L., 1984. Large volcanic debris avalanches: Characteristics of source areas, deposits, and associated eruptions. J. Volcanol. Geotherm. Res. 22, 163–197.
Skinner Jr., J.A., Tanaka, K.L., 2007. Evidence for and implications of sedimentary diapirism and mud volcanism in the southern Utopia highland–lowland boundary plain, Mars. Icarus 186, 41–59.
Smith, D.E. et al., 2001. Mars Orbiter Laser Altimeter: Experiment summary after the first year of global mapping of Mars. J. Geophys. Res. 106, 23689–23722.
Squyres, S.W. et al., 2004. The Spirit rover's Athena science investigation at Gusev Crater, Mars. Science 305, 794–799.
Sullivan, R., Thomas, P., Veverka, J., Malin, M., Edgett, K.S., 2001. Mass movement slope streaks imaged by the Mars Orbiter Camera. J. Geophys. Res. 106, 23607–23633. doi:10.1029/2000JE001296.
Tanaka, K.L., Dohm, J.M., Lias, J.H., Hare, T.M., 1998. Erosional valleys in the Thaumasia region of Mars: Hydrothermal and seismic origins. J. Geophys. Res. 103, 31407–31419.
Tanaka, K.L., Skinner Jr., J.A., Hare, T.M., 2005. Geologic map of the northern plains of Mars. USGS Scientific Investigations Map SIM-2888, Scale 1:15,000,000.
Valentino, G.M., Cortecci, G., Franco, E., Stanzione, D., 1999. Chemical and isotopic compositions of minerals and waters from Campi Flegrei volcanic system, Naples, Italy. J. Volcanol. Geoth. Res. 91, 329–344.
Varekamp, J.C., 2004. Copahue volcano: A modern terrestrial analog for the opportunity landing site. Eos 85 (41), 401–407.
Varekamp, J.C., Pasternack, G.B., Rowe Jr., G.L., 2000. Volcanic lake systematics II. Chemical constraints. J. Volcanol. Geotherm. Res. 97, 161–179.
Varekamp, J.C., Ouimette, A., Kreulen, R., 2004. The magmato-hydrothermal system of Copahue volcano, Argentina. In: Wanty, R.B., Seal, R.R. (Eds.), Proceedings of the 11th Water Rock Interaction Symposium, pp. 215–218.
Warren-Rhodes, K. et al., 2007. Searching for microbial life remotely: Satellite-to-rover habitat mapping in the Atacama Desert, Chile. J. Geophys. Res. 112, G04S05. doi:10.1029/2006JG000283.
Williams, P., Pigram, C., Dow, D., 1984. Melange production and the importance of shale diapirism in accretionary terrains. Nature 309, 145–146.
Wilson, S.A., Howard, A.D., Moore, J.M., Grant, J.A., 2007. Geomorphic and stratigraphic analysis of Crater Terby and layered deposits north of Hellas basin, Mars. J. Geophys. Res. 112, E08009. doi:10.1029/2006JE002830.
Yen, A.S. et al., 2008. Hydrothermal processes at Gusev Crater: An evaluation of Paso Robles class soils. J. Geophys. Res 113, E06S10. doi:10.1029/2007JE002978.